Alteration and self-reversal in oceanic basalts

Pavel V. Doubrovine[1] and John A. Tarduno[1]

Received 25 April 2006; revised 7 August 2006; accepted 25 August 2006; published 3 November 2006.

[1] We report on magnetic properties and compositions of titanomaghemites from moderately to highly oxidized basalts recovered at nine drilling sites in the Pacific Ocean. These new data, together with similar data sets, allow us to test compositional fields of titanomaghemite that could carry self-reversed components of natural remanent magnetization above room temperature. These compositions have been proposed on the basis of theoretical considerations of cation distributions during ionic reordering associated with low-temperature oxidation (maghemitization). The data indicate that very high oxidation states ($z \geq 0.9$) and relatively high Ti contents ($x \geq 0.6$) are needed to produce natural self-reversed components; this compositional range is much more limited than predicted. The severe restrictions on compositions and oxidation state strongly suggest that self-reversed magnetizations should not be a general feature of the magnetization carried by oceanic basalt. Instead, the formation of self-reversed components may signify unusual conditions, such as extreme fluid flow and iron removal, which could result in the required oxidation states while maintaining stability of the cation-deficient titanomaghemite lattice structure.

Citation: Doubrovine, P. V., and J. A. Tarduno (2006), Alteration and self-reversal in oceanic basalts, *J. Geophys. Res.*, *111*, B12S30, doi:10.1029/2006JB004468.

> Self-reversal by ionic re-ordering occurs during extreme low-temperature oxidation of high-Ti (large x) titanomagnetites... Reversals of this sort may possibly occur in highly maghemitized submarine basalts, although this remains to be demonstrated.
>
> *Dunlop and Özdemir* [1997]

1. Introduction

[2] The possibility of that some oceanic basalts could carry a self-reversed chemical remanent magnetization (CRM) has been discussed for the last 40 years [e.g., *Verhoogen*, 1956, 1962; *O'Reilly and Banerjee*, 1966; *O'Reilly*, 1983]. *Verhoogen* [1956, 1962] suggested that self-reversal could be produced during extreme low-temperature oxidation of titanomagnetite by ionic reordering. Seafloor weathering of basalt is ubiquitous and characterized by low-temperature oxidation, or maghemitization, of titanomagnetites [e.g., *Bleil and Petersen*, 1983]. On this basis, self-reversals might be expected in oxidized oceanic basalts [e.g., *Dunlop and Özdemir*, 1997]. However, a clear example was not immediately found in natural oceanic rocks and the process received relatively little subsequent attention. Renewed interest in ionic reordering in titanomaghemite has been motivated by the discovery of prominent self-reversed magnetization components in some samples of Late Cretaceous pillow lavas from Detroit Seamount in the northwestern Pacific Ocean [*Doubrovine and Tarduno*, 2004].

[3] Titanomaghemite, a metastable cation-deficient ferrimagnetic spinel produced during low-temperature oxidation of titanomagnetite, is represented by

$$Fe^{3+}_{[2-2x+z(1+x)]R}Fe^{2+}_{(1+x)(1-z)R}Ti^{4+}_{xR}\square_{3(1-R)}O^{2-}_{4}$$

where $R = 8/[8 + z(1 + x)]$, $\square$ denotes a cation vacancy, x ($0 \leq x \leq 1$) is a compositional parameter, and z ($0 \leq z \leq 1$) is the degree of oxidation [*O'Reilly*, 1984]. This formula assumes the oxidation by the addition of oxygen. This process may well occur above the Fe-redox boundary in oceanic sediments [*Smirnov and Tarduno*, 2000]. In oceanic basalts, however, oxidation occurs by the removal iron due to the interaction with seawater and/or seawater-derived fluids [*O'Reilly*, 1984; *Furuta*, 1993; *Dunlop and Özdemir*, 1997]. In this paper we will use the x and z as compositional parameters defined by *O'Reilly* [1984], irrespective of the mechanism of oxidation.

[4] Spontaneous magnetization (M_s) of stoichiometric titanomagnetite of any composition x is dominated by the collective magnetic moment of iron cations residing in the octahedrally coordinated sites of the inverse spinel lattice (B magnetic sublattice). According to the theoretical model of maghemitization process developed by *O'Reilly and Banerjee* [1966], low-temperature oxidation occurs first at the expense of octahedral Fe^{2+}, resulting in a decrease of the B sublattice magnetic moment (M_B). At higher oxidation states, when octahedral Fe^{2+} is exhausted, oxidation proceeds at slower rates at the expense of Fe^{2+} residing in tetrahedral sites (A magnetic sublattice). However, cation vacancies created at tetrahedral sites migrate into the octahedral sublattice, which is accomplished by the dif-

[1]Department of Earth and Environmental Sciences, University of Rochester, Rochester, New York, USA.

0148-0227/06/2006JB004468$09.00

fusion of iron cations from B to A sites. This process of cation vacancy redistribution is termed "ionic reordering" [*Verhoogen*, 1956, 1962]. Ionic reordering results in a further decrease of M_B and in a slight increase of the A sublattice magnetic moment (M_A), lowering the value of M_s ($M_s = |M_B - M_A|$). At a certain critical degree of oxidation, when the tetrahedral magnetic moment becomes dominating ($M_A/M_B > 1$), this process may transform a single domain (and perhaps pseudosingle domain) CRM carried by titanomaghemite into an antipodal CRM due to intrinsic self-reversal of M_s. In the case when the initial CRM pseudomorphs the primary thermoremanent magnetization (TRM) of titanomagnetite (e.g., for single and pseudosingle-domain titanomaghemite carriers [*Marshall and Cox*, 1971; *Özdemir and Dunlop*, 1985; *Brown and O'Reilly*, 1988]), a self-reversal of natural remanent magnetization (NRM) would be observed.

[5] *Verhoogen* [1962] reported the theoretical compositional range of titanomaghemite capable of carrying a self-reversed CRM from a consideration of cation distribution in titanomaghemite. Later, *O'Reilly and Banerjee* [1966] showed that the cation distribution used by Verhoogen is unrealistic and restricted the self-reversal field of titanomaghemite to oxidation states significantly higher than those in the original Verhoogen's model. *O'Reilly and Banerjee* [1966] also suggested that high oxidation degrees required to produce a self-reversal by ionic reordering may be unreachable at low ambient temperatures (e.g., room temperature or seafloor temperatures). High temperatures which may otherwise lead to high degrees of oxidation are incompatible with the stability of the cation-deficient structure of titanomaghemite.

[6] *Schult* [1968, 1971] suggested that low-temperature oxidation of titanomagnetite and attendant ionic reordering should produce a Q → P → L → N → Q′ sequence of the $M_s(T)$ curve types [*Néel*, 1948]. This model predicts that titanomaghemites which undergo self-reversal by ionic reordering should exhibit either N-type thermomagnetic behavior with temperatures of magnetic compensation above room temperature or Q′-type behavior.

[7] In recent studies of submarine basalts recovered by the Deep Sea Drilling Project (DSDP) and the Ocean Drilling Program (ODP) several cases of N-type thermomagnetic behavior of highly oxidized titanomaghemite have been reported [e.g., *Wang*, 2002; *Matzka et al.*, 2003; *Doubrovine and Tarduno*, 2004; *Carvallo et al.*, 2004; *Doubrovine and Tarduno*, 2006]. Similar behavior has also been documented in some continental basalts [*Schult*, 1965, 1968, 1976; *Krása*, 2003] and basalts associated with subduction zones [*Nishida and Sasajima*, 1974]. In only two studies, however, were N-type behavior above room temperature and self-reversed magnetizations carried by titanomaghemite observed: (1) in oxidized alkali basalt of Miocene age from Steinberg at Meensen, Germany [*Schult*, 1976], and (2) in the pillow lavas of Detroit Seamount of the northwestern Pacific Ocean [*Tarduno et al.*, 2003]. Specifically, partial self-reversal components have been documented in pillow basalts from Site 883 and the nearby Site 1204 [*Doubrovine and Tarduno*, 2004]. Evidence for self-reversal in titanomaghemite was also found in alkali basalts of Oligocene age from New South Wales, Australia [*Hoffman*, 1982], but thermomagnetic properties of titanomaghemite were not investigated.

[8] The compositions of self-reversing titanomaghemite from Detroit Seamount [*Doubrovine and Tarduno*, 2004] were constrained to very high oxidation states ($z \geq 0.8$, $0.65 \leq x \leq 0.86$), consistent with theoretical estimates [e.g., *O'Reilly and Banerjee*, 1966]. Later work on the basalts from DSDP sites 307 and 166, which do not carry self-reversed CRM components, further constrained the compositional field of self-reversing titanomaghemite to oxidation states $z \geq 0.9$ [*Doubrovine and Tarduno*, 2005, 2006]. In this paper we present new paleomagnetic, compositional and rock magnetic data obtained from moderately to highly oxidized submarine basalts collected from nine DSDP and ODP sites in the Pacific Ocean and discuss their implications for self-reversal carried by titanomaghemite in oceanic basalts.

2. Samples

[9] On the basis of visual core descriptions and petrographic observations, moderately to highly altered submarine basalts recovered from nine sites in the Pacific Ocean were selected for study (Figure 1 and Table 1). Samples were collected from azimuthally unoriented cores at the West Coast and Gulf Coast ODP core repositories. All samples are tholeiitic basalts, including those which have been erupted at or near mid-ocean ridges (sites 170, 303A, 304, 801C, and 1173B) and the basalts from an oceanic plateau (Ontong Java Plateau, sites 803D, 1183A, 1185A, 1185B, and 1187A). The majority of basalts are Cretaceous in age (~90–135 Ma, seven sites, Table 1); the two remaining sites represent middle Miocene (~15 Ma, Site 1173B) and Middle Jurassic (~160–168 Ma, Site 801C) oceanic crust. Brief descriptions of these basalts are given in the auxiliary materials, whereas detailed information can be found in the initial reports of the DSDP (Legs 17 and 32) and the ODP (legs 129, 130, 185, 192, and 196).[1]

[10] Basalts selected for study exhibit prominent alteration characteristics suggestive of prolonged interaction with seawater, seawater-derived low-temperature fluids and/or mixtures of seawater and low-temperature hydrothermal fluids. Alteration is characterized by partial or complete replacement of groundmass and phenocrysts by clays (e.g., celadonite, montmorillonite, saponite, chlorite), Fe-oxyhydroxide (oxidizing conditions) or pyrite (more reducing environment). Alteration under the oxidizing conditions is most prominent in oxidation haloes developing along fractures/veins or pillow rims.

[11] Short basement sections (a few to a few tens of meters, sites 170, 303A, 304, 803D, 1173B) show moderate to high degrees of alteration consistent with "normal" conditions of seafloor weathering (i.e., dominant oxidation by interaction with seawater at bottom seawater temperature). Two sections from Ontong Java Plateau (the 126-m-thick upper basalt group from Site 1185 and the 136-m-thick section from Site 1187A) show high degrees of pervasive low-temperature alteration by seawater-derived fluids under highly oxidizing conditions and high water/

[1] Auxiliary material data sets are available at ftp://ftp.agu.org/apend/jb/2006jb004468. Other auxiliary material files are in the HTML.

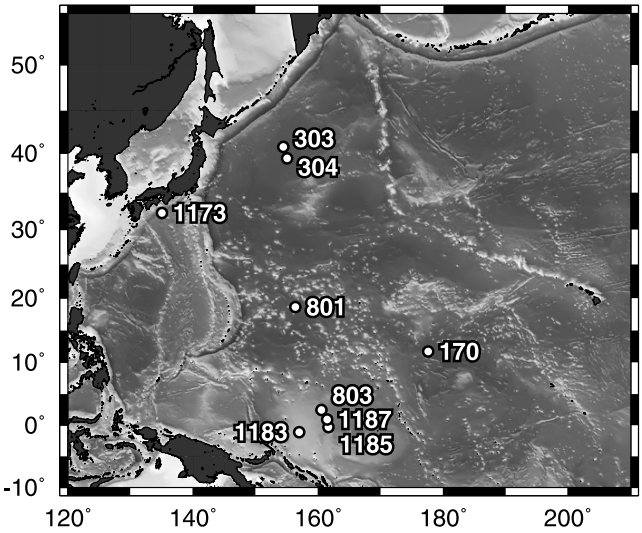

Figure 1. Locations of DSDP and ODP sites selected for study.

rock ratios [*Mahoney et al.*, 2001]. These sections were sampled at irregular intervals. Several to several tens of samples were collected from each site.

[12] The remaining two sections (sites 801C and 1183A), as well as the lower basalt group from Site 1185B, show various alteration types ranging from pervasive alteration under anoxic/suboxic conditions to prominent black, brown and olive-brown haloes concentrated along veins, suggesting highly oxidizing conditions [*Banerjee and Honnorez*, 2004; *Alt and Teagle*, 2003]. These sections were sampled selectively in the intervals where significant low-temperature oxidation could be inferred from secondary mineral assemblages.

3. Magnetic Mineralogy

[13] Examination of polished thin sections using a reflected light microscope and a Leo 982 scanning electron microscope (SEM) at the University of Rochester showed that the opaque mineralogy of basalts from the nine sites is dominated by titanomagnetite altered by various degrees to titanomaghemite (Figure 2). For the majority of samples (sites 303A, 801C, 803D, 1183A, 1185, 1187A, and 1173B), titanomaghemite grains are small (<1 μm to ~20–30 μm), with skeletal to subhedral shapes typical for rapidly quenched basalt lavas (Figures 2a–2g). Cracks observed in some of the grains appear to be shrinkage cracks, formed to accommodate the decrease in lattice parameter with the increasing degrees of low-temperature oxidation. Large cracks propagating through the adjacent silicate matrix were sometimes seen; these may have been introduced during the preparation of thin sections.

[14] In one sample from Site 801C (sample 801C-7R1-110, Figure 2b) we observed partial replacement of titanomaghemite by some amorphous/poorly crystalline Ti-rich material (probably a mixture of sphene or titanium oxide with clays). The replacement is probably related to extensive low-temperature hydrothermal alteration, which has been described from the uppermost portion of tholeiitic basalt section of Site 801C [*Lancelot et al.*, 1990; *Alt and Teagle*, 2003]. In the second sample from Site 801C (sample 801C-11R3-116, Figure 2c), no replacement features were seen; titanomaghemite grains in this sample are similar to fine-grained titanomaghemites from other sites.

[15] Larger grain sizes were observed in samples of massive lava flows from sites 170 and 304 (Figures 2h and 2i). Titanomagnetite grains from the Site 304 basalt (sample 304-16R1-111, Figure 2i) are up to ~100 μm in size and seemingly unaltered, with skeletal or subhedral shapes and few cracks. This basalt sample is probably the freshest among those we have studied. Titanomaghemites from the Site 170 basalt (sample 170-16R1-39) show a bimodal grain size distribution with (1) unusually large (up to ~200 μm), skeletal to subhedral grains showing prominent (up to ~500 nm thick) shrinkage cracks (Figure 2i) and (2) smaller grains (less than a few tens of μm in size) with similar shapes and alteration features. The presence of shrinkage cracks suggest that, despite large grain sizes, titanomagnetite in the Site 170 basalt is significantly oxidized. Another unusual characteristic of the Site 170 basalt

Table 1. DSDP and ODP Sites Selected for Study

Leg	Site	Latitude, N	Longitude, E	Basement Age[a]	Reference
DSDP 17	170	11°48.0′	177°37.00′	Early Cretaceous (≥100 Ma)	*Winterer et al.* [1973]
DSDP 32	303A	40°48.50′	154°27.07′	Early Cretaceous (~130 Ma)	*Larson et al.* [1975]
DSDP 32	304	39°20.27′	155°04.19′	Early Cretaceous (~133–134 Ma)	*Larson et al.* [1975]
ODP 129, 185	801C	18°38.54′	156°21.59′	Middle Jurassic (~160–169 Ma)	*Lancelot et al.* [1990] and *Plank et al.* [2000]
ODP 130	803D	2°25.98′	160°32.46′	Late Cretaceous (~90 Ma) or Early Cretaceous (~122–125 Ma)[b]	*Kroenke et al.* [1991] *Tarduno et al.* [1991]
ODP 192	1183A	−1°10.62′	157°00.90′	Early Cretaceous (≥118 Ma)	*Mahoney et al.* [2001]
ODP 192	1185A, B	−0°21.46′	161°40.06′	Cretaceous (94–112, ≥112 Ma)	*Mahoney et al.* [2001]
ODP 192	1187A	0°56.55′	161°27.08′	Early Cretaceous (≥118 Ma)	*Mahoney et al.* [2001]
ODP 196	1173B	32°14.68′	135°01.48′	middle Miocene (~15–16 Ma)	*Mikada et al.* [2002]

[a]Numerical ages are according to the timescale of *Gradstein et al.* [2004].

[b]Two age models have been proposed for Site 803 and the Ontong Java Plateau. On the basis of magnetostratigraphy and stratigraphic sections on and surrounding the plateau [*Tarduno et al.*, 1989; *Tarduno*, 1990], it has been suggested that most of the plateau formed in a brief (<3 m.y.) period of the Early Aptian [*Tarduno et al.*, 1991]. Alternatively, radiometric age data from Site 803, which yield a nominal age of 90 Ma, have been used to suggest that the plateau formed in at least two discrete intervals [*Mahoney et al.*, 1993]. Recent radiometric age data of Leg 192 (Site 1184A, 123.5 ± 1.6 Ma [*Chambers et al.*, 2004]; sites 1183, 1185, 1186 and 1187, 121.5 ± 1.7 Ma [*Parkinson et al.*, 2002]) support the model of *Tarduno et al.* [1991], implying that the 90 Ma age from Site 803 represents an alteration age.

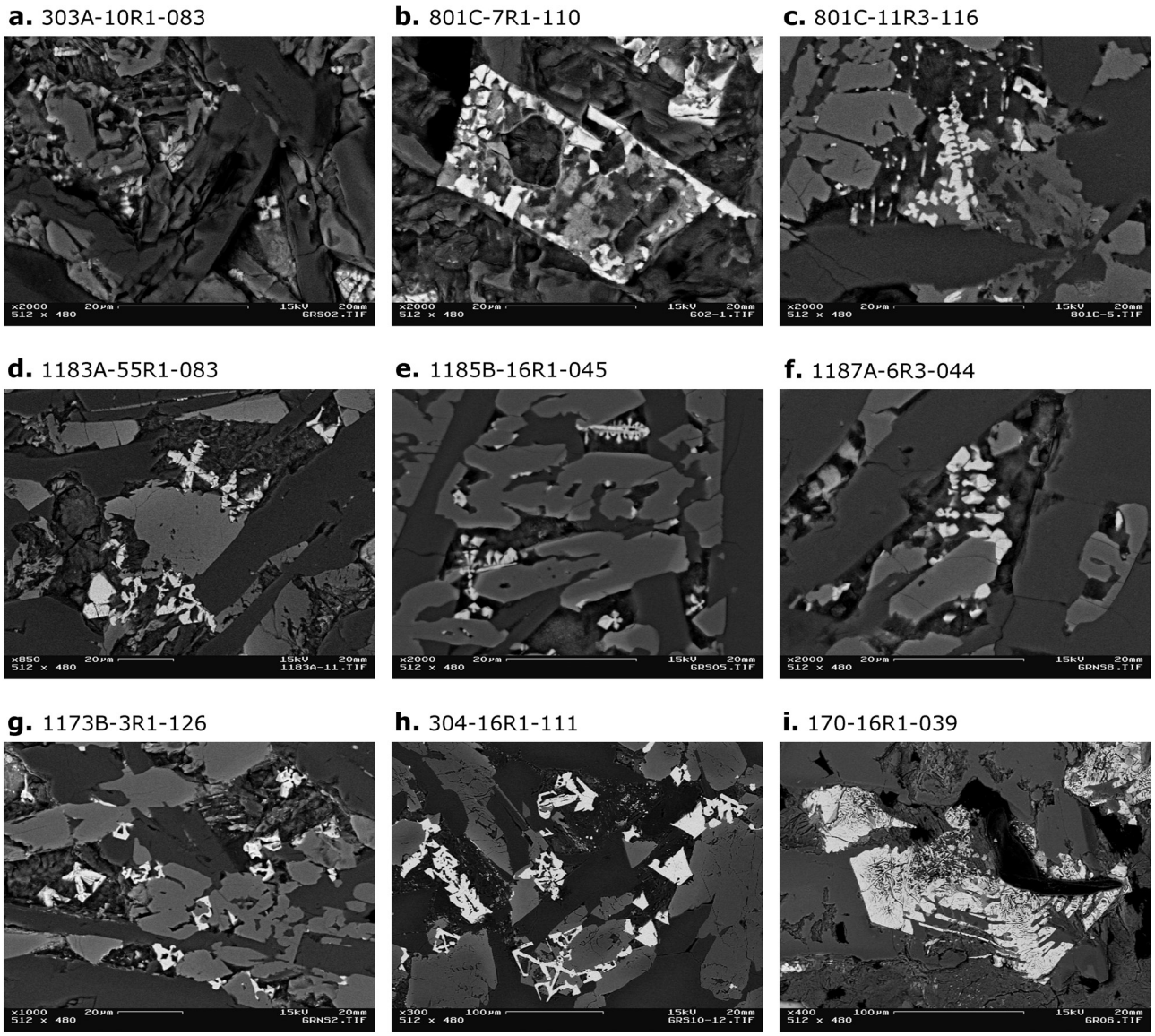

Figure 2. Backscattered electron images of titanomaghemite grains.

is the presence of abundant ilmenite grains (or rather high-Ti hemoilmenite, Fe_{2-y} Ti_y O_3, see section 6.1) coexisting with titanomaghemite.

[16] In summary, the opaque mineralogy described from reflected light and SEM observations is typical for weathered submarine basalts, with a few exceptions, as discussed above. In all samples, magnetic carriers are nonstoichiometric titanomagnetites (titanomaghemites); their compositions and oxidation states will be discussed in section 6.

4. Demagnetization Data

[17] One hundred fifty samples were selected for thermal demagnetization experiments (auxiliary material Table S1). At least four samples were taken from each of the short basalt sequences (sites 170, 303A, 304 and 1173B). Twelve to forty five samples per site were taken from the longer sections (sites 801C, 803D, 1183A, 1185, and 1187A) to ensure proper representation of these variably altered sequences. Samples, cut as 1 cm cubes, were thermally demagnetized at 25°C steps within a 50–625°C range using an ASC TD-48 thermal demagnetization device; measurements of the NRM remaining after each demagnetization step were made using a 2G DC SQUID magnetometer. Demagnetization data were plotted as orthogonal vector projections (Figure 3) and analyzed using principal component analysis (PCA) [*Kirschvink*, 1980]. We used the following criteria for definition of the directions of characteristic remanent magnetization (ChRM): (1) at least four demagnetization steps should define the ChRM, (2) demagnetization trajectories of the ChRM should point toward the origin in orthogonal vector plots, and (3) the maximum angular deviation (MAD) [*Kirschvink*, 1980] of ChRM data from the PCA fit should not exceed 15°.

[18] The majority of samples showed a well-defined ChRM (Figures 3a–3e). Some of these (e.g., those from sites 170, 304, and 1173B) showed the removal of a normal polarity overprint at low unblocking temperatures

(Figures 3a, 3c, and 3d). Normal polarity overprints were most prominent in data from Site 1173B (as also noted by the Leg 197 Shipboard Scientific Party that analyzed these basalts, see [*Mikada et al.*, 2002]). Such overprints are typically observed in oceanic basalts and are usually interpreted as viscous magnetizations acquired in the recent geomagnetic field, drill string-induced overprints or a combination of the two.

[19] An exception to this well-defined behavior was presented by the samples from Site 801C. One half of the Site 801C samples showed demagnetization of spurious NRM components (with various inclinations and polarity). Often, the demagnetization data up to ~400–450°C did not define a trajectory going to the origin of orthogonal vector plots. At higher demagnetization temperatures, erratic changes of magnetization were observed. In these cases the ChRM could not be defined.

[20] Another exception was observed in a few samples from sites 303A, 801C, 803D, 1183A, and 1185B and from the majority of the samples from Site 1187A (Figures 3f, 3g, and 3i). In these samples, the NRM directions remained stable at all thermal treatment levels. The NRM intensity decreased upon heating to ~200–250°C, then increased (usually between ~200–250°C and 300–350°C), and thereafter decreased to ~550–600°C, where samples were demagnetized. This behavior can be formally described as sequential demagnetization of three nearly antiparallel NRM components with distinct unblocking temperatures: two of the same polarity unblocking at low and high temperatures, respectively, and one of the opposite polarity demagnetizing at intermediate temperatures.

[21] To check whether these components can be resolved in AF demagnetization data, thermally untreated sister samples (i.e., 1 cm cubes taken from the same core intervals) of the several samples showing antiparallel components in thermal demagnetization experiments were demagnetized using a Sapphire Instruments SI-4 AF demagnetizer. AF demagnetization (performed at 5 and 10 mT increments up to 150–190 mT maximum applied field) showed no indication of multiple antiparallel components. A simple univectorial decay of the NRM was observed in all cases (Figures 3h and 3j). The ChRM directions isolated above ~10–15 mT and fit by principal component analysis were indistinguishable from those defined from thermal demagnetization data at high unblocking temperatures (Figures 3g–3j). Similar demagnetization behavior was previously reported from basalts collected at sites 807, 1187A, and 307 by *Mayer and Tarduno* [1993], *Riisager et al.* [2003] and *Doubrovine and Tarduno* [2005], respectively. All authors argued that the increase in the NRM intensity seen in the ~200–350°C range of unblocking temperatures in thermal demagnetization

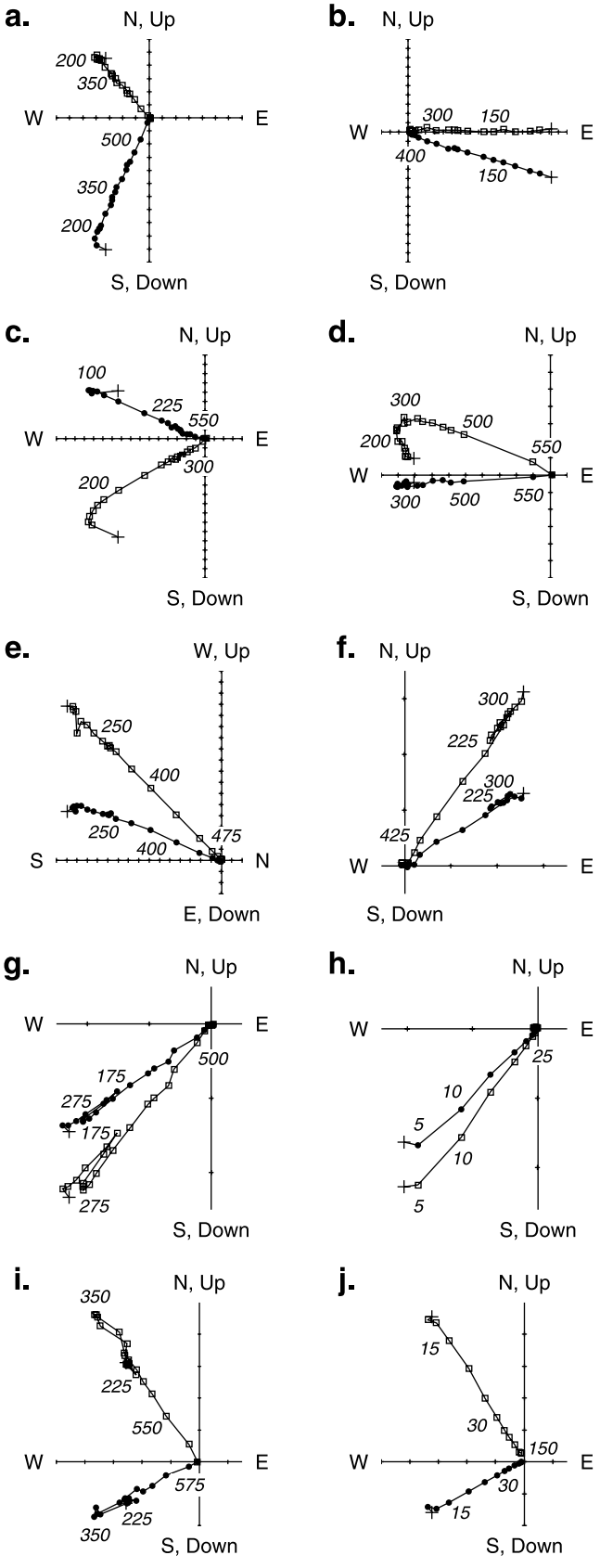

Figure 3. Examples of orthogonal vector plots of (a–g and i) stepwise thermal and (h and j) AF demagnetization. Open squares, projection of magnetization on a vertical plane; solid circles, projection of the magnetization on a horizontal plane (note that ODP samples recovered by rotary drilling are azimuthally unoriented). Numbers next to data represent thermal (°C) or AF (mT) treatment levels. Samples 170-16R1-025 (Figure 3a), 303A-9R1-128 (Figure 3b), 304-15R2-003 (Figure 3c), 1173B-3R1-126 (Figure 3d), 1185B-14R1-054 (Figure 3e), 803D-70R1-021 (Figure 3f), 801C-11R3-116 (Figures 3g and 3h), and 1187A-3R5-063 (Figures 3i and 3j).

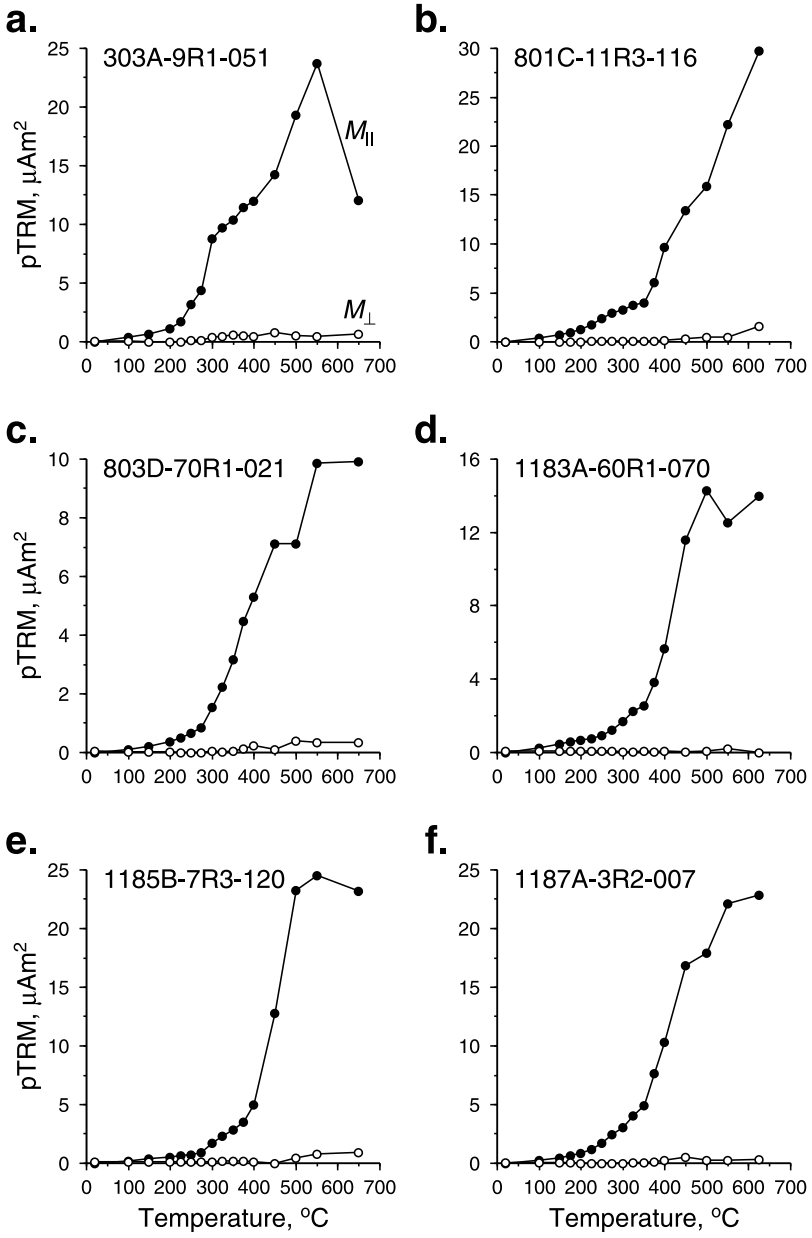

Figure 4. Acquisition of pTRM for basalt samples showing apparent antiparallel NRM components in thermal demagnetization data. $M_{||}$, magnetization acquired parallel to the applied field; $M_{\perp}$, magnetization acquired perpendicular to the field.

data is probably related to the processes of thermally-induced alteration of titanomaghemite during laboratory heating. This is consistent with our comparisons of the thermal and AF demagnetization data [see also *Riisager et al.*, 2003].

[22] Although the similarities with the results of earlier studies are striking, they do not necessarily mean that the increases in the NRM intensity seen in thermal demagnetization experiments are an artifact of thermally induced sample alteration and that the alternative explanation by partial self-reversal of NRM due to ionic reordering in titanomaghemite should be rejected solely on the basis of AF demagnetization data. Our earlier results from the Detroit Seamount basalts [*Doubrovine and Tarduno*, 2004] suggest that the coercivities of the self-reversed NRM components can greatly overlap with those of the CRM which mimics the original TRM direction. When the intensity of self-reversed CRM is small, which may be the case for our samples, the self-reversed magnetization can be masked below the resolution of AF demagnetization data by a dominant CRM which has not undergone self-reversal. Experiments on acquisition of partial thermoremanent magnetization (pTRM) proved to be successful for the discrimination between these two possibilities [*Doubrovine and Tarduno*, 2004, 2005] and will be discussed in section 5.

5. The pTRM Acquisition Experiments

[23] The idea of this experiment is based on the hypothesis of *Schult* [1968, 1971], who suggested that titanoma-

Table 2. Compositions of Titanomaghemite[a]

Site	Core	Section	Interval, cm	x	x_{subst}	$(\delta_{Al})_{max}$	$(\delta_{Mg})_{max}$	$a \pm \Delta a$, Å	z	$z_{ATM60/10}$
170	16R	1	39–41	0.50–0.66	0.49–0.62	0.06–0.15	≤0.07	8.388 ± 0.005	0.83	0.69
303A	9R	1	51–53	*0.68–0.75*				8.380 ± 0.006	0.89	0.72
303A	10R	1	83–85	*0.66–0.82*				8.380 ± 0.005	0.89	0.72
304	16R	1	111–113	0.63–0.68	0.61–0.66	0.08–0.11	n.d.	8.441 ± 0.004	0.55	0.51
801C	11R	3	116–119	0.47–0.67	0.44–0.64	0.10–0.16	0.03–0.10	8.386 ± 0.005	0.84	0.70
803D	68R	4	42–44	*0.61–0.73*				8.373 ± 0.003	0.91	0.76
803D	70R	1	21–23	*0.57–0.75*				8.356 ± 0.007	0.96	0.85
1183A	55R	1	83–85	0.61–0.68	0.58–0.65	0.11–0.15	n.d.	8.390 ± 0.003	0.84	0.68
1185B	8R	1	133–135	*0.26–0.53*				8.352 ± 0.005	0.96	0.87
1185B	16R	1	45–47	0.30–0.56	0.27–0.54	0.13–0.22	≤0.09	8.347 ± 0.006	0.97	0.89
1187A	3R	5	63–65	0.50–0.52	0.47–0.48	0.11–0.20	0.06–0.09	8.356 ± 0.006	0.95	0.85
1187A	6R	3	44–46	0.36–0.56	0.34–0.54	0.09–0.18	≤0.07	8.352 ± 0.005	0.96	0.87
1173B	3R	1	126–128	0.67–0.77	0.61–0.69	0.10–0.13	n.d.	8.413 ± 0.007	0.74	0.60

[a]Parameters are as follows: x, composition parameter of titanomaghemite estimated from the EDS data assuming no cation substitution; x_{subst}, minimum value of x for cation-substituted titanomaghemite; $(\delta_{Al})_{max}$, $(\delta_{Mg})_{max}$, maximum values of the degree of Al and Mg substitution, respectively; a, Δa are the lattice parameter and its 95% confidence limits; z, oxidation parameter of titanomaghemite estimated from the comparison with data of *Readman and O'Reilly* [1972]; $z_{ATM60/10}$, oxidation parameter estimated from the comparison with data from the ATM60/10 titanomaghemite series of *Özdemir and O'Reilly* [1982]. The n.d. denotes the cases when the concentrations of Mg were below the detection limits. The compositional parameters in italics are approximate values based on the EDS data where significant matrix contamination precluded accurate quantification (see text).

ghemite in which the remanent magnetization undergoes a self-reversal by ionic reordering should exhibit "anomalous" N-type thermomagnetic behavior with compensation temperature above room temperature. If a significant population of titanomaghemite grains with such thermomagnetic behavior is present in the sample, and if their blocking temperatures are above the compensation point and below the inversion temperature [*Özdemir*, 1987], these grains are capable of acquiring a self-reversed pTRM. Because these grains carry a self-reversed CRM, the temperature range where the self-reversed pTRM is blocked should be similar to the unblocking temperatures of the self-reversed NRM component. This exact situation was observed for the samples of Detroit Seamount basalt in which a self-reversed CRM component was carried by titanomaghemite with N-type thermomagnetic properties [*Doubrovine and Tarduno*, 2004].

[24] pTRM acquisition experiments were performed on thermally untreated sister samples of the basalt samples yielding the apparent antiparallel NRM components in thermal demagnetization data. Samples were first demagnetized by alternating field (up to 150–190 mT) to remove the NRM, and then heated to, and cooled from, the sequentially increasing temperatures in the presence of a 40 μT magnetic field oriented parallel to the z sample axis in an ASC TD-48 thermal demagnetization device. The pTRM acquired after each step was measured with a 2G DC SQUID magnetometer.

[25] All samples showed the acquisition of normal pTRM only (i.e., pTRM in the direction of applied field, Figure 4). In the ~200–350°C range, where the apparent antiparallel NRM components were commonly unblocking (section 4), we often observed increases in the slope of pTRM acquisition curves, suggesting more efficient blocking of normal pTRM, as opposed to the acquisition of self-reversed pTRM expected for the N-type magnetic particles carrying a true self-reversed CRM [*Doubrovine and Tarduno*, 2004]. Further increases in slope of pTRM curves above 300–400°C probably correspond to the inversion of titanomaghemite.

[26] The pTRM acquisition data suggest that the increases in the NRM intensity observed in the intermediate range of unblocking temperatures (~200–350°C) do not result from the unblocking of true self-reversed CRM components. In sections 6 and 7, we will discuss the compositions and rock magnetic properties of titanomaghemites from studied basalt samples, which may provide keys for understanding the origin of the apparent antiparallel NRM components observed in thermal demagnetization data.

6. Compositions of Titanomaghemite

6.1. Energy-Dispersive Spectrometry and *x* Values

[27] Cation contents and x values of titanomaghemite were estimated through X-ray energy-dispersive spectrometry (EDS) on single grains of titanomaghemite using the Leo 982 SEM equipped with an EDAX Phoenix EDS system at the University of Rochester. Thirteen polished, gold-coated thin sections of the representative basalt samples were studied (Table 2). Backscattering electron (BSE) imaging was used to identify the oxide grains in thin sections. Energy-dispersive X-ray spectra were measured at a 15 kV accelerating voltage, which is optimal for the excitation of the Fe K shell, and then analyzed with EDAX SEM Quant version 3.2 software. A detailed description of the quantification procedure used to calculate relative cation abundances in titanomaghemite is published elsewhere [*Doubrovine and Tarduno*, 2005].

[28] Ten to twelve grains of titanomaghemite were analyzed in each thin section to ensure proper representation of the magnetic carriers and to assess the variability of the titanomaghemite composition in the sample. Because of the limited spatial resolution imposed by the size of the electron beam interaction volume (estimated to be ~1.5 μm in titanomaghemite at 15 keV acceleration voltage), X-ray spectra were measured from grains (or areas within grains) larger than 3–5 μm in size, which appeared homogeneous in BSE images. However, in some cases, when the magnetic fraction consisted of very small titanomagnetite grains (i.e., two samples from Site 303A, two samples from Site 803D,

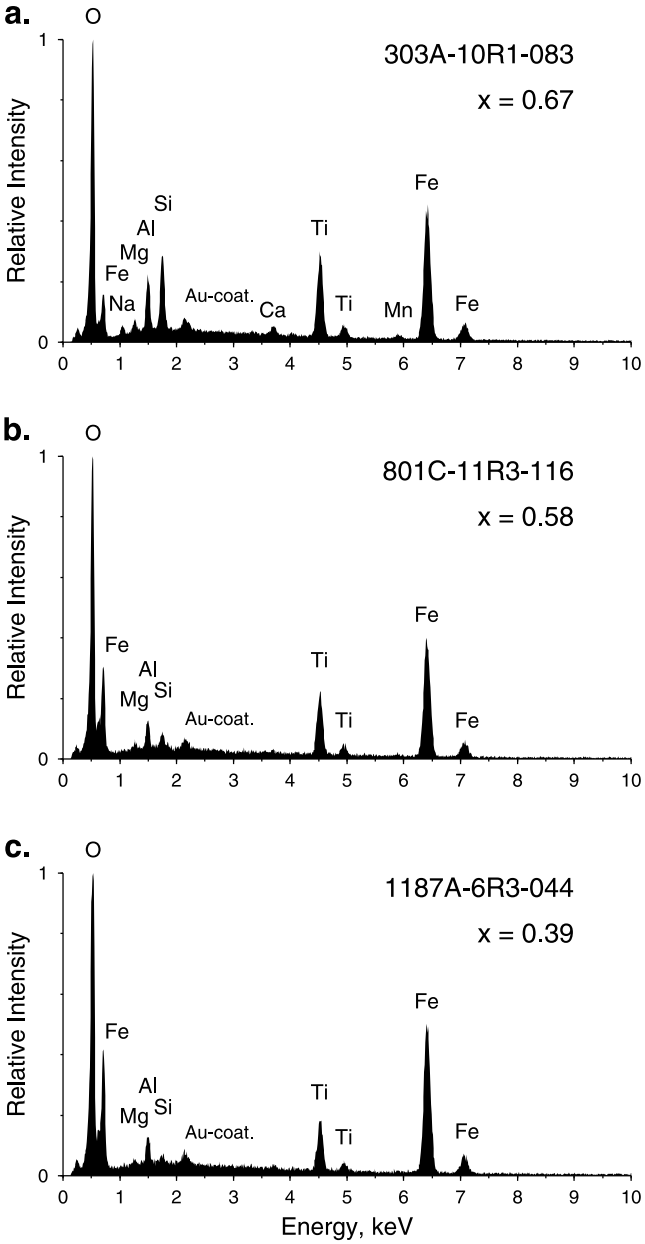

Figure 5. Examples of energy-dispersive X-ray spectra measured on single grains of titanomaghemite.

and one sample from Site 1185B, Table 2), we were not able to find grains large enough to yield a spectrum that we can expect to be free of significant contamination from the surrounding silicate matrix (e.g., Al, Si, Mg, Ca, Na, K) (Figure 5a). Fe/Ti ratios from these small grains (≤ 2 μm) were estimated assuming that the Fe and Ti $K\alpha$ peaks in the spectra come exclusively from titanomaghemite, ignoring the effect of matrix contamination. The values for these samples thus are only crude estimates of the actual Fe/Ti ratios.

[29] Another problem in analyzing EDS data from small grains (several to few tens μm in size, in which the electron beam interaction volume is fully contained within the grain) was the potential presence of a "contamination signal" from characteristic X-ray fluorescence originating from the surrounding matrix material. (Note that characteristic X-ray fluorescence is produced by interaction between the primary X rays excited within the electron beam interaction volume and the material within the X-ray fluorescence range, which is at least several tens times larger than the size of the interaction volume [*Goldstein et al.*, 1992].) However, because no Ti was found in the matrix material from qualitative EDS analyses, it was possible to attribute the Fe and Ti $K\alpha$ lines in measured spectra to titanomaghemite and to obtain accurate estimates of the (Fe/Ti) ratios. The x values of titanomaghemite in studied basalt samples were calculated using a simple relationship:

$$x = \frac{3}{1 + (\mathrm{Fe/Ti})} \tag{1}$$

where (Fe/Ti) is the atomic ratio estimated from EDS data. The observed ranges are given in Table 2.

[30] Equation (1) assumes that titanomaghemite is a pure Fe-Ti oxide. Natural titanomaghemites in submarine basalts, however, often contain small amounts of impurity cations (among which Al and Mg are most common) substituting for the Fe cations. Cation-substituted titanomaghemite can be represented by

$$\mathrm{Fe}_{(3-x-\delta)R}\mathrm{Ti}_{xR}M_{\delta R}\square_{3(1-R)}\mathrm{O}_4$$

where M stands for the impurity cation and δ is the degree of cation substitution.

[31] In the ED spectra of titanomaghemite grains from analyzed basalts, small Al (or Al and Mg) peaks were observed for all samples (Figures 5b and 5c). Titanomaghemite grains from Site 1173B basalt (sample 1173B-3R1-126) also showed the presence of minor amounts of Mn. It is not clear, however, whether these peaks originate from titanomaghemite or from the X-ray fluorescence effect in the neighboring silicate minerals. Small Si peaks of comparable intensity were commonly observed together with the peaks from Al and Mg. Because Si is not usually present in significant quantities in natural titanomagnetites [e.g., *Creer and Ibbetson*, 1970; *Zhou et al.*, 1999], this observation suggests that the X-ray fluorescence in the silicate matrix may significantly contribute to the measured intensities of Al and Mg peaks.

[32] Assuming that the entire Al and Mg signal comes from titanomaghemite, we calculated the degrees of cation substitution and the values of x for cation-substituted titanomaghemite (x_{subst}) using

$$\delta_{\mathrm{Al}} = \frac{3}{1 + (\mathrm{Fe/Al}) + (\mathrm{Ti/Al}) + (\mathrm{Mg/Al})} \tag{2}$$

$$\delta_{\mathrm{Mg}} = \frac{3}{1 + (\mathrm{Fe/Mg}) + (\mathrm{Ti/Mg}) + (\mathrm{Al/Mg})} \tag{3}$$

$$x_{\mathrm{subst}} = \frac{3}{1 + (\mathrm{Fe/Ti}) + (\mathrm{Al/Ti}) + (\mathrm{Mg/Ti})} \tag{4}$$

where all cation/cation ratios are atomic ratios estimated from the quantification of EDS data. Because it is not

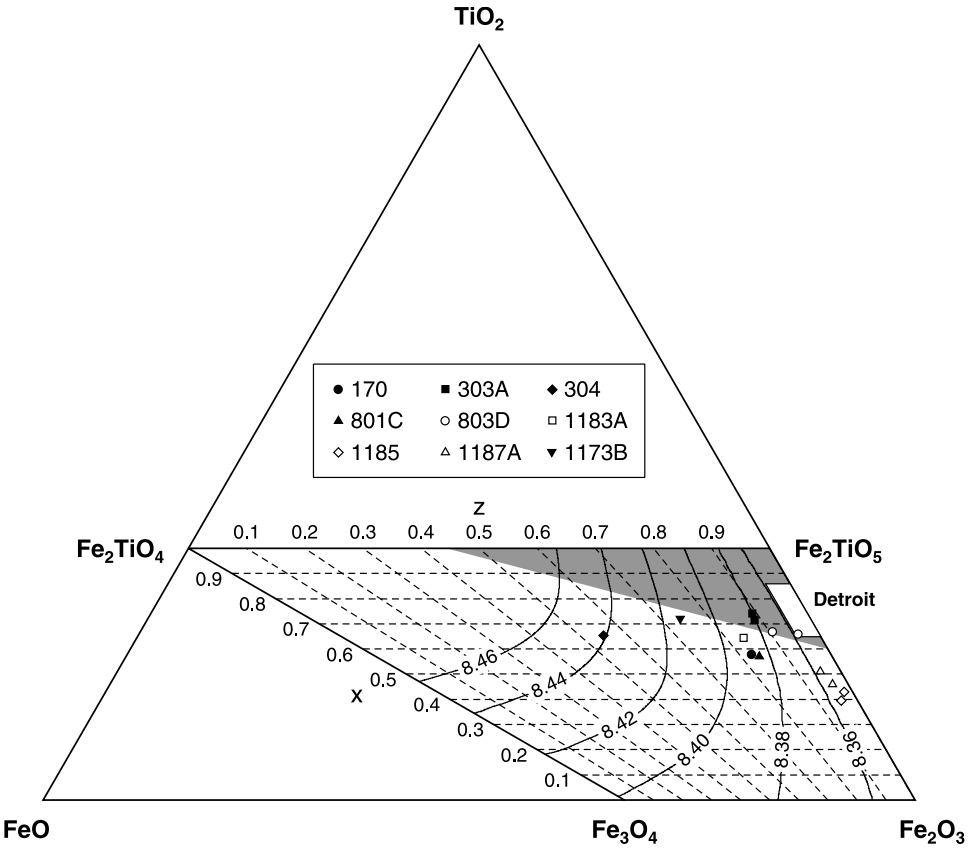

Figure 6. TiO_2-FeO-Fe_2O_3 ternary diagram. Symbols show the average compositions of titanomaghemite calculated assuming no cation substitution (Table 2). Gray area is the self-reversal field of *O'Reilly and Banerjee* [1966]. White area is the compositional range of self-reversing titanomaghemite from Detroit Seamount basalt [*Doubrovine and Tarduno*, 2004]. Contours of constant lattice parameter for titanomaghemite (Å) are from *Readman and O'Reilly* [1972].

possible to separate the potential sources of Al and Mg, these estimates represent the upper limits of the degrees of cation substitution (δ_{Al}, δ_{Mg}) and the lower limit of x_{subst} (Table 2).

[33] The estimates of x (or x_{subst}) values obtained from basalt samples from sites 170, 303A, 304, 801C, 803D, 1183A, and 1173B overlap with a 0.5–0.8 range of x values typically observed in mid-ocean ridge basalts [e.g., *Furuta*, 1993]. Titanomaghemite grains in samples from sites 1185B and 1187A on Ontong Java Plateau showed lower x values ranging from 0.26 to 0.56. These atypically low values of x are consistent with the bulk chemistry of the basalts from Site 1185 (upper basalts sequence) and 1187A, which is characterized by relatively primitive compositions with low Ti contents, distinct from the compositions of other basalts recovered from Ontong Java Plateau (e.g., sites 803D and 1183A) [*Mahoney et al.*, 2001].

[34] Cation contents and y values of hemoilmenite observed in the basalt sample from Site 170 (sample 170-16R1-39) were estimated using a relationship

$$y = \frac{2}{1 + (\mathrm{Fe/Ti})} \tag{5}$$

where (Fe/Ti) is the atomic ratio in hemoilmenite calculated from the EDS data. Several large hemoilmenite grains ($\geq$50 μm) were analyzed in this sample and a range of y values from 0.88 to 0.91 was observed. Hemoilmenite of this composition is paramagnetic at room temperature and does not contribute into the remanent magnetization [e.g., *Dunlop and Özdemir*, 1997].

6.2. X-Ray Powder Diffraction: Lattice Parameters and Oxidation States

[35] To estimate the lattice parameter (a) of titanomaghemite, X-ray powder diffraction (XPD) analyses were performed on magnetic separates using a Philips Multipurpose diffractometer (MPD) at the University of Rochester. Magnetic separates were prepared from the same basalt samples for which the x values were measured from the EDS analyses (section 6.1, Table 2). All magnetic separates yielded XPD spectra with prominent diffraction lines characteristic for the face-centered cubic lattice of titanomaghemite. Lattice parameters calculated from the six major lines are given in Table 2.

[36] The comparison of the lattice parameters and x values with data from well characterized synthetic titanomaghemites [*Readman and O'Reilly*, 1972; *Nishitani and Kono*, 1983] suggests high oxidation states of titanomaghemite for the majority of samples (Figure 6 and Table 2). The lowest values of a, and hence the highest degrees of oxidation, were observed for titanomaghemites from the

Table 3. Site-Mean Inclinations of ChRM[a]

Site	n	I, deg	$\Delta I_{95\%}$, deg	k	s, deg
170	12	25.7	1.8	553.36	3.4
303A	7	3.7	5.1	161.96	6.4
304	4	23.0	23.9	25.86	15.9
803D	13	−44.2	4.2	94.03	8.4
1183A	16	−41.5	6.6	29.93	14.8
1185	30	−42.0	3.5	50.77	11.4
1187A	45	−41.7	2.0	101.13	8.1
1173B	3	−23.5	17.0	146.46	6.7

[a]Parameters are as follows: n, number of samples used to calculate site-mean inclination; I, $\Delta I_{95\%}$, site-mean inclination and its 95% uncertainty, respectively; k, best estimate of precision parameter [*McFadden and Reid*, 1982]; s, directional angular dispersion.

Site 803D, 1185B and 1187A basalts ($z \geq 0.9$). Titanomaghemites in the basalt samples from sites 170, 303A, 801C, and 1183A showed somewhat lower oxidation states, in a 0.8–0.9 range of z. Titanomaghemites from sites 304 and 1173B showed the highest values of lattice parameter (Table 2), corresponding to $z = 0.55$ and $z = 0.74$, respectively.

[37] The estimates of z given above were calculated assuming no cation substitution in titanomaghemite. Data from synthetic Al- and Mg-substituted titanomagnetites and titanomaghemites show that the lattice parameter generally decreases with increasing degrees of cation substitution [*Richards et al.*, 1973; *O'Donovan and O'Reilly*, 1977; *Özdemir and O'Reilly*, 1981]. Because it is likely that titanomaghemites from our basalt samples are slightly Al- and Mg-substituted (see section 6.1), the z values calculated assuming no cation substitution probably slightly overestimate the actual values of oxidation parameter.

[38] To assess the effect of cation substitution on calculated z values, we compared our lattice parameter data with the data of *Özdemir and O'Reilly* [1981] for the ATM60/10 series (x = 0.6, δ_{Al} = 0.1) of synthetic Al-substituted titanomaghemites. The oxidation states of ATM60/10 titanomaghemite ($z_{ATM60/10}$) corresponding to the values of lattice parameter measured from magnetic separates are given in Table 2. These values are not directly applicable to the oxidation states of our titanomaghemites because (1) only the upper limits of δ_{Al} are available from the EDS data (as was discussed in section 6.1) and the actual values of δ_{Al} may significantly differ from 0.1, (2) the effect of Mg substitution (if any) was not taken into account and (3) the x values differ from 0.6 in most cases (Table 2). We note, however, that the degrees of Al substitution $\delta_{Al} \leq 0.1$ are typical for titanomaghemite from submarine basalts [e.g., *Furuta*, 1993; *Zhou et al.*, 1999]. We also note that Mg substitution has a much less pronounced and opposite effect on the lattice parameter of titanomaghemite (i.e., slightly increasing a for $\delta_{Mg} \leq 0.15$) [*O'Donovan and O'Reilly*, 1977] as compared with Al substitution. The maximum degrees of Mg substitution estimated from EDS analyses were always significantly lower than (or negligible compared to) the Al substitution in our samples (Table 2). Also, it has been shown that the lattice parameters of pure synthetic titanomaghemites with different Ti contents converge to the same value at high oxidation states (a = ~8.34 Å at z = 1 for $0 \leq x \leq 1$ [*Readman and O'Reilly*, 1972; *Nishitani and Kono*, 1983]) and the lattice parameter of highly oxidized titanomaghemite is only weakly dependent on x. Therefore we believe that the calculated values of $z_{ATM60/10}$ provide a reasonable approximation of the minimum value of oxidation parameter. The true oxidation parameters are likely to be between the values of $z_{ATM60/10}$ and those estimated from the comparison with data of *Readman and O'Reilly* [1972] (Table 2).

7. Rock Magnetism

7.1. Magnetic Hysteresis Properties

[39] Magnetic hysteresis loops were measured at room temperature on small basalt chips in a 1 T maximum applied field (using a Princeton Measurements Corporation Alternating Gradient Force Magnetometer at the University of Rochester). The saturation magnetization of the ferromagnetic component (M_s), coercivity (H_c) and the ratio of saturation remanent magnetization (M_{rs}) to M_s were estimated from the loops corrected for paramagnetic slope. The coercivity of remanence (H_{cr}) was calculated from backfield demagnetization of the saturation remanence.

[40] Two different approaches were used to perform the paramagnetic slope correction. The first approach was the standard procedure of subtracting a linear trend with the average slope of the loop above 70% of the maximum field from the magnetization versus field data. This procedure (which will be referred to as slope-tangent approximation) assumes that the ferromagnetic component is fully saturated at and above 0.7 T. However, it was suggested recently that titanomaghemites from submarine basalts tend to be undersaturated in fields as high as 1 T and that insufficient saturation can lead to the underestimated values of M_s (and overestimated M_{rs}/M_s ratios) inferred using the slope-tangent approximation [*Matzka et al.*, 2003; *Fabian*, 2006].

[41] In the case of significant undersaturation, a more accurate estimate of M_s can be obtained by fitting the reversible part of the hysteresis loop (the high-field region where the upper and lower branches of the loop coincide) with an idealized curve describing the approach to saturation. We have used an explicit formulation of the approach to the saturation law [*von Dobeneck*, 1996]:

$$M(H) = M_s + \kappa_{pd} H - \frac{\alpha}{H} \tag{6}$$

where M is the total magnetization in the applied field H, κ_{pd} is the susceptibility of paramagnetic and diamagnetic components, and α is a constant ($\alpha > 0$). The fit parameters (M_s, κ_{pd} and α) were calculated using a least squares regression algorithm and the estimate of κ_{pd} was then used to perform the slope correction. A more detailed description of this procedure is published elsewhere [*Doubrovine and Tarduno*, 2006].

[42] The values of M_s estimated using the regression procedure (equation (6)) were consistently higher than those calculated using the slope-tangent approximation, even for the "magnetically soft" samples with low M_{rs}/M_s and high H_{cr}/H_c ratios (auxiliary material Table S2). This observation suggests that all samples were undersaturated in the 1 T field. The degree of undersaturation, defined as

$$u = \frac{M_{s2} - M_{s1}}{M_{s2}} 100\% \tag{7}$$

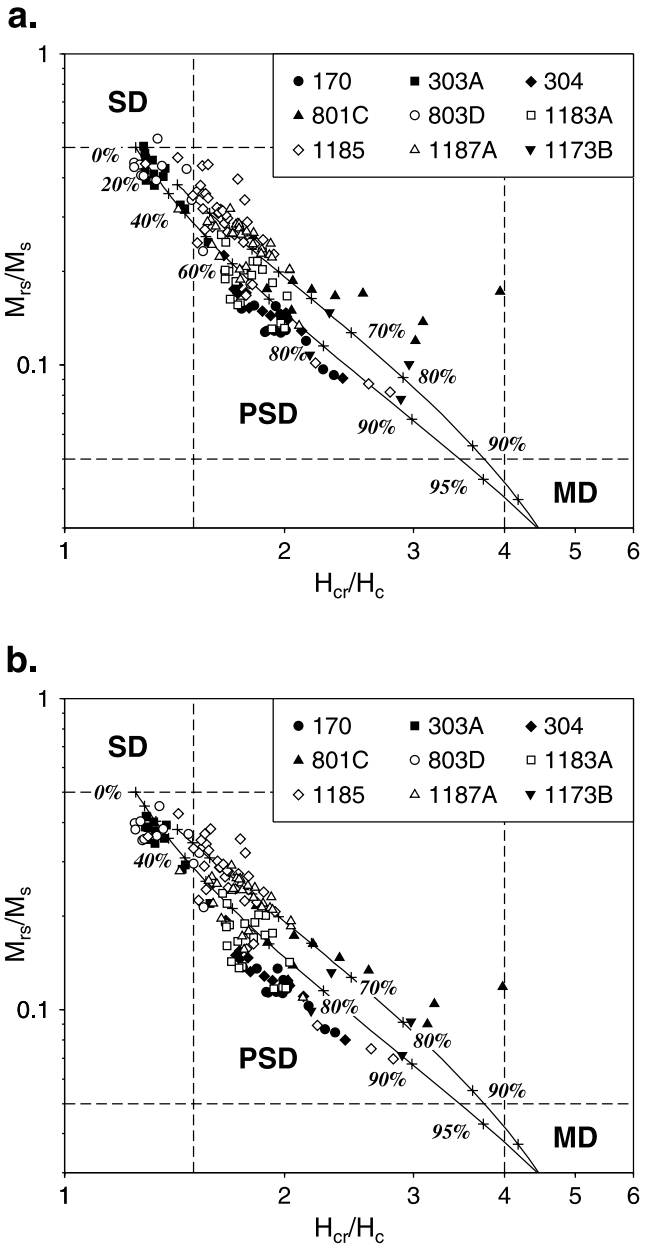

Figure 7. Summary of magnetic hysteresis parameters on Day diagrams [*Day et al.*, 1977]. Thin solid lines are theoretical curves for mixtures of SD and MD grains after *Dunlop* [2002]. SD, single-domain; PSD, pseudosingle-domain; MD, multidomain. (a) Values calculated using the slope-tangent approximation; (b) values calculated using the regression procedure (see text).

where M_{s1} and M_{s2} are the estimates of M_s calculated using the slope-tangent approximation and the regression method, respectively, were between ~8% and 15% for the majority of samples (auxiliary material Table S2). These values are lower than those reported from other submarine basalts [*Matzka et al.*, 2003; *Fabian*, 2006]. We note, however, that the samples studied by *Matzka et al.* [2003] and *Fabian* [2006] exhibit extremely high M_{rs}/M_s ratios, close to the theoretical limit for uniaxial, single-domain magnetic carriers ($M_{rs}/M_s \approx 0.5$); our samples have significantly lower values, mostly within the ~0.1–0.4 range (assuming that the regression method yields correct values for M_s).

[43] The M_{rs}/M_s versus H_{cr}/H_c data show the bulk magnetic properties of the studied basalt samples ranging from nearly single domain (SD) to pseudosingle-domain (PSD) behavior [*Day et al.*, 1977; *Dunlop*, 2002] (Figure 7). Hysteresis data generally follow the single-domain to multidomain (SD-MD) mixing trends of *Dunlop* [2002], with the exception of the data from the Site 801C basalts, which show a departure from the SD-MD trend in the direction of higher H_{cr}/H_c values, suggesting the presence of superparamagnetic particles.

[44] The highest values of M_{rs}/M_s and H_{cr}/H_c ratios, close to the SD-PSD boundary (Figure 7), were observed in basalts from sites 303A and 803D. The SD to PSD properties are consistent with the small grain sizes (usually $\leq$5–10 μm) and high oxidation states of titanomaghemite [*Moskowitz*, 1980] observed in these basalts (section 6.2). Basalts from sites 1185 and 1187A showed slightly lower M_{rs}/M_s and higher H_{cr}/H_c values in the PSD range (Figure 7). Because the sizes of titanomaghemite grains and their oxidation states are similar to those from sites 303A and 803D, the difference is probably related to lower x values (section 6.1). The remaining samples (sites 170, 304, 801C, 1173B, and 1183A) showed PSD behavior (Figure 7). Bulk hysteresis properties of these basalts are probably dominated by large titanomaghemite grains (few tens to few hundreds μm) with few magnetic domains. This interpretation is consistent with the theoretical estimates of magnetic domain state for titanomaghemites with moderate to high oxidation states [*Moskowitz*, 1980].

7.2. High-Field Thermomagnetic Behavior

[45] Temperature dependences of saturation magnetization were studied by measuring hysteresis loops at 10 or 20 K temperature increments on representative basalt samples at the Institute for Rock Magnetism, University of Minnesota. A Princeton Measurements Corporation Vibrating Sample Magnetometer (VSM) with an attached cryostat was used for measurements from 10 K to 400 K (−263 to 127°C) and a VSM equipped with a high-temperature furnace was used for measurements between 300 and 620 K (27 and 347°C). Hysteresis loops were measured first during warming a sample from cryogenic temperatures (10 or 20 K) to 340 K, then during a 300 K → 620 K → 300 K heating-cooling cycle, and then during cooling from 340 K to 10 or 20 K. A maximum applied field of 1 T was used throughout the experiment.

[46] $M_s(T)$ dependences were obtained from the combined low- and high-temperature hysteresis data. For each hysteresis loop the paramagnetic slope correction was performed using both the slope-tangent approximation and the regression procedure described in section 7.1. The fitting of the hysteresis data with the regression curve (equation (6)) was performed in the region $\mu_0 H_{tr} \leq \mu_0 H \leq 1$ T, where H_{tr} is a threshold value chosen to be $15H_c$ if 0.2 T $\leq 15\mu_0 H_c \leq$ 0.7 T, 0.2 T if $15\mu_0 H_c <$ 0.2 T, or 0.7 T if $15\mu_0 H_c >$ 0.7 T (H_c was estimated from the slope-tangent approximation). The loops measured above ~100–130 K on the samples from sites 303A and 803D, and above ~50–70 K for the samples from the remaining sites, were closed at 0.7 T. At lower temperatures, however, the loops

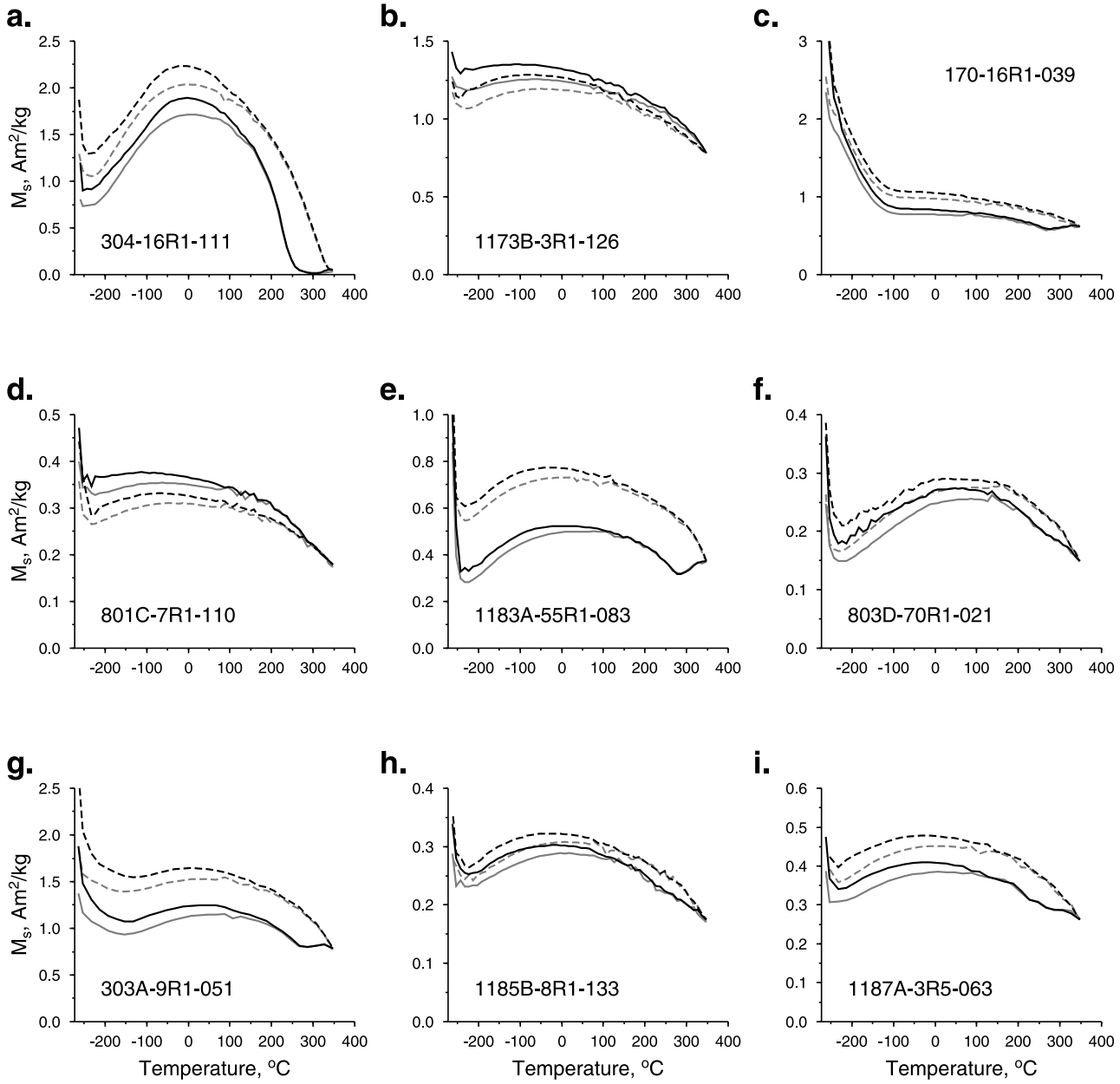

Figure 8. Examples of $M_s(T)$ curves obtained by measuring hysteresis loops versus temperature. Gray curves, estimates of M_s calculated using the slope-tangent approximation; black curves, estimates of M_s calculated using the regression procedure; solid lines, heating curves; dashed lines, cooling curves.

did not close at 0.7 T. In these cases, we calculated nominal estimates of M_s by averaging the values estimated separately from the upper and lower branches of the hysteresis loop. Because the approach to saturation regime was not reached in the 0.7–1 T region at very low temperatures, these M_s estimates are only tentative.

[47] $M_s(T)$ curves showed P-type thermomagnetic behavior for the most samples (Figure 8). For the basalt samples in which titanomaghemite has "normal" x values ($0.5 \leq x \leq 0.8$, all sites except sites 1185B and 1187A), we did not observe a simple Q $\rightarrow$ P $\rightarrow$ L $\rightarrow$ N evolution of the $M_s(T)$ curve types with the increasing oxidation states. The freshest titanomaghemite from Site 304 basalt ($z \approx 0.5$) showed well-expressed P-type behavior with a maximum of M_s slightly below room temperature (Figure 8a). More oxidized titanomaghemite from Site 1173B ($z \approx 0.7$) showed much less developed P-type maximum of M_s below room temperature, with overall shape of $M_s(T)$ curve approaching to that characteristic for Q-type behavior (Figure 8b). Similar "flat" P-type/Q-type curves were observed from samples of the Site 170 and 801C basalts in which the oxidation degrees of titanomaghemite were estimated to be $z \approx 0.8$ (Figures 8c and 8d). In the two samples from Site 170 (samples 170-16R1-39 and 170-16R2-72) we observed steep increases in saturation magnetization at low temperatures, corresponding to magnetic ordering of high-Ti hemoilmenite below $\sim$140 K (-133°C, Figure 8c). This temperature is in a good agreement with Curie temperature

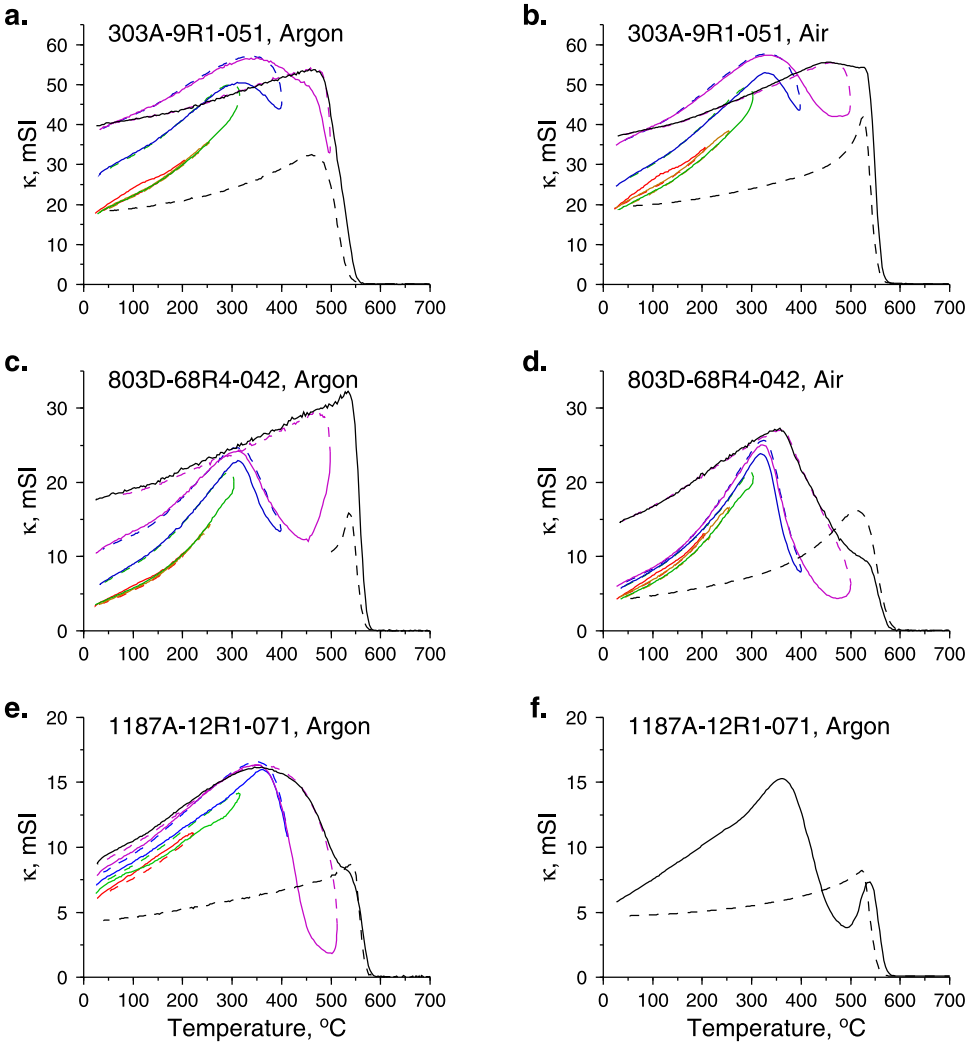

Figure 9. Low-field thermomagnetic curves measured (a–e) in sequential heating-cooling cycles and (f) in a single thermomagnetic run on whole rock samples. Solid lines, heating curves; dashed lines, cooling curves. Colors denote paired heating-cooling cycles.

expected for hemoilmenite with $y \approx 0.9$ [*Nagata*, 1961], consistent with the y values determined through the EDS analyses of hemoilmenite grains from Site 170 basalt (section 6.1). Interestingly, samples from Site 1183A, in which titanomaghemite appears to have similar oxidation degree and x values as in Site 170 and 801C basalts, showed more convex $M_s(T)$ curves (Figure 8e). (Note that the sharp increases in M_s observed below 30 K (−243°C) in this and many other samples are probably related to the magnetic ordering of Fe-rich clays and/or ilmenite, which are paramagnetic at room temperature and do not contribute into the NRM.)

[48] Titanomaghemites with the highest oxidation degrees from the Site 803D basalt showed well defined P-type $M_s(T)$ curves (Figure 8f). A broad minimum of $M_s(T)$ was observed at ~110–130 K in two samples from Site 303A (samples 303A-9R1-42 and 303A-9R1-51, Figure 8g), suggesting N-type magnetic carriers with low compensation temperatures. Alternatively, a decrease in M_s at low temperatures may be attributed to a magnetic phase (e.g., high-Ti hemoilmenite) with the Curie temperature of ~110–130 K. Although we did not observe ilmenite in polished thin sections of the Site 303A basalt, we can not completely rule this possibility out. The remaining samples of the Site 303A basalt showed P-type curves, similar to those from the Site 803D samples (Figure 8f).

[49] The basalts from sites 1185 and 1187A, in which titanomaghemites have distinctly lower x values ($0.26 \leq x \leq 0.56$) and very high oxidation states ($z \geq 0.9$) (section 6), showed "flat" P-type curves with broad M_s maxima slightly below room temperature (Figures 8h and 8i).

[50] $M_s(T)$ curves for all samples showed slight to moderate degrees of irreversibility upon heating to 620 K (347°C), consistent with the initiation of the inversion in titanomaghemite. In some samples, the onset of inversion was clearly visible between 250–300°C (e.g., Figures 8e and 8g). These temperatures are slightly lower than the ~300–460°C inversion temperatures observed from synthetic Al-substituted titanomaghemites with moderate to high degrees of oxidation ($z > 0.5$) [*Özdemir*, 1987]. We note, however, that this discrepancy may originate from the differences in heating rates (the heating rates in our experi-

ments were ~5 min per 20 K temperature increment or ~3.5 min per 10 K increment) and/or from different criteria used to define the inversion temperature. We will further discuss the inversion of titanomaghemite in section 7.3.

7.3. Low-Field Thermomagnetic Data

[51] Temperature dependences of magnetic susceptibility ($\kappa(T)$) were measured on whole rock samples using an AGICO KLY-4S kappabridge equipped with a high-temperature furnace at the University of Rochester. Because we were specifically interested in the alteration of titanomaghemite during laboratory heating and its effect on the NRM intensity, this experiment was focused on samples showing the apparent antiparallel magnetization components in thermal demagnetization data (section 4). Susceptibility measurements were performed in consecutive heating-cooling cycles with sequentially increasing maximum heating temperatures (200, 250, 300, 400, 500 and 700°C) in air and argon (Figures 9a–9e).

[52] In the first two heating-cooling cycles, upon heating to 200°C and 250°C, all $\kappa(T)$ curves showed nearly reversible behavior, with very small degrees of irreversibility, more prominent in the curves measured in air. Upon further heating to 300°C, all curves showed significant irreversibility, except the curve measured in air on one sample from Site 1187A (sample 1187A-6R3-44), which was reversible. Similar or larger degrees of irreversibility were observed upon heatings to 400 and 500°C. After the final heating-cooling cycle, upon heating to 700°C, titanomaghemite was completely inverted, probably forming an iron-rich spinel inversion product with Curie temperatures between 560 and 580°C. Irreversibility of thermomagnetic curves suggest the onset of titanomaghemite inversion at or slightly below 300°C (i.e., in a 250–300°C range) for all studied samples. This range is in excellent agreement with the inversion temperatures estimated from the $M_s(T)$ measurements (section 7.2).

[53] To see what inversion temperatures would be obtained if we were to estimate the onset of inversion from a single thermomagnetic run (as, for example, was done in study of *Özdemir* [1987]), we measured $\kappa(T)$ curves from a few samples in continuous heating-cooling experiments, run up to 700°C in argon. A typical result, illustrated in Figure 9f, was the observation of two "humps" in heating curves: the first hump at ~300–400°C, and the second at ~450–550°C. Following the definitions of *Özdemir* [1987], the temperature corresponding to the beginning of titanomaghemite inversion would be determined from the ascending shoulder of the second hump to be (~500°C). The first hump would be interpreted as a Hopkinson peak of titanomaghemite, corresponding to Curie temperature of ~460°C. On the other hand, the $\kappa(T)$ curves measured from the same sample in sequential heating-cooling cycles (Figure 9e) suggest that the inversion begins at temperatures ≤300°C and that 500°C is the temperature where metastable Fe-rich spinel product of inversion starts to grow rapidly, on a timescale comparable with the time between individual measurements of κ during a continuous run. This example provides a clear explanation of the apparent discrepancy between our estimates of the inversion temperature and those reported from synthetic titanomaghemites [*Özdemir*, 1987].

[54] Comparing thermomagnetic curves measured in air and in argon, a clear difference in the degree of irreversibility can be noted for the curves measured in 400°C and 500°C cycles (Figures 9a–9d). When samples were heated in argon, the Curie temperature of the presumed metastable Fe-rich spinel inversion product increased continuously in sequential heating-cooling cycles. When measured in air, this increase in Curie temperature was slower, occurring between 400 and 500°C. A similar, but more pronounced effect was observed in sequential $\kappa(T)$ measurements on basalt samples from DSDP Site 307 [*Doubrovine and Tarduno*, 2005]. In the basalts from Site 307, larger degrees of irreversibility were observed in first heating-cooling cycles (200 and 250°C) and stabilization of Curie temperature at ~400°C was seen in the 400 and 500°C cycles for the susceptibility curves measured in air. Because the inversion temperature of titanomaghemite increases with the increasing oxidation state [e.g., *Özdemir*, 1987], the stabilization of Curie temperature was interpreted as an evidence for additional single-phase oxidation of titanomaghemite during laboratory heating in air, which is consistent with the irreversibility of thermomagnetic curves in first heating-cooling cycles. Although the irreversibility of $\kappa(T)$ curves upon heating to 200°C and 250°C in our samples is noticeably smaller than that seen in data from the Site 307 basalts, and no clear stabilization of Curie temperature was observed, the similarities of the two data sets suggest that some single-phase oxidation may have occurred in our samples during heatings in air to 200–300°C.

7.4. Heating Experiments on Magnetic Separates

[55] To further evaluate relative importance of single-phase oxidation and inversion of titanomaghemite, we performed heating experiments on magnetic separates collected from two samples: 803D-68R4-42 and 1187A-6R3-44. These samples were chosen because they represent titanomaghemites with "normally high" and low x values, respectively, and high oxidation states (Table 2); both samples showed antiparallel magnetization components in thermal demagnetization experiments. Each magnetic separate was divided into three parts. One part was not heated. The second part was heated in air (using the AGICO KLY-4S kappabridge) to 300°C (sample 803D-68R4-42) or to 325°C (sample 1187A-6R3-44). The third part was heated in air to 700°C. The heating rate (~10°C/min) and the time at the maximum temperature (15 min) were chosen to simulate the conditions during the thermal demagnetization experiments. The lower heating temperatures (300°C and 325°C) were chosen to match the maximum unblocking temperature of the "reversed" magnetization component observed in thermal demagnetization data (auxiliary material Table S1). X-ray powder diffraction spectra were then measured on fresh and heated separates using the Philips MPD.

[56] Fresh samples and samples heated to 300–325°C showed nearly identical X-ray diffraction patterns, with prominent reflections characteristic of cubic face-centered titanomaghemite lattice (Figures 10a and 10b). The calculations of lattice parameter from measured patterns showed slightly lower values of a for the heated samples. For sample 803D-68R4-42, lattice parameter decreased from 8.373 ± 0.003 Å (fresh sample) to 8.370 ± 0.004 Å (after

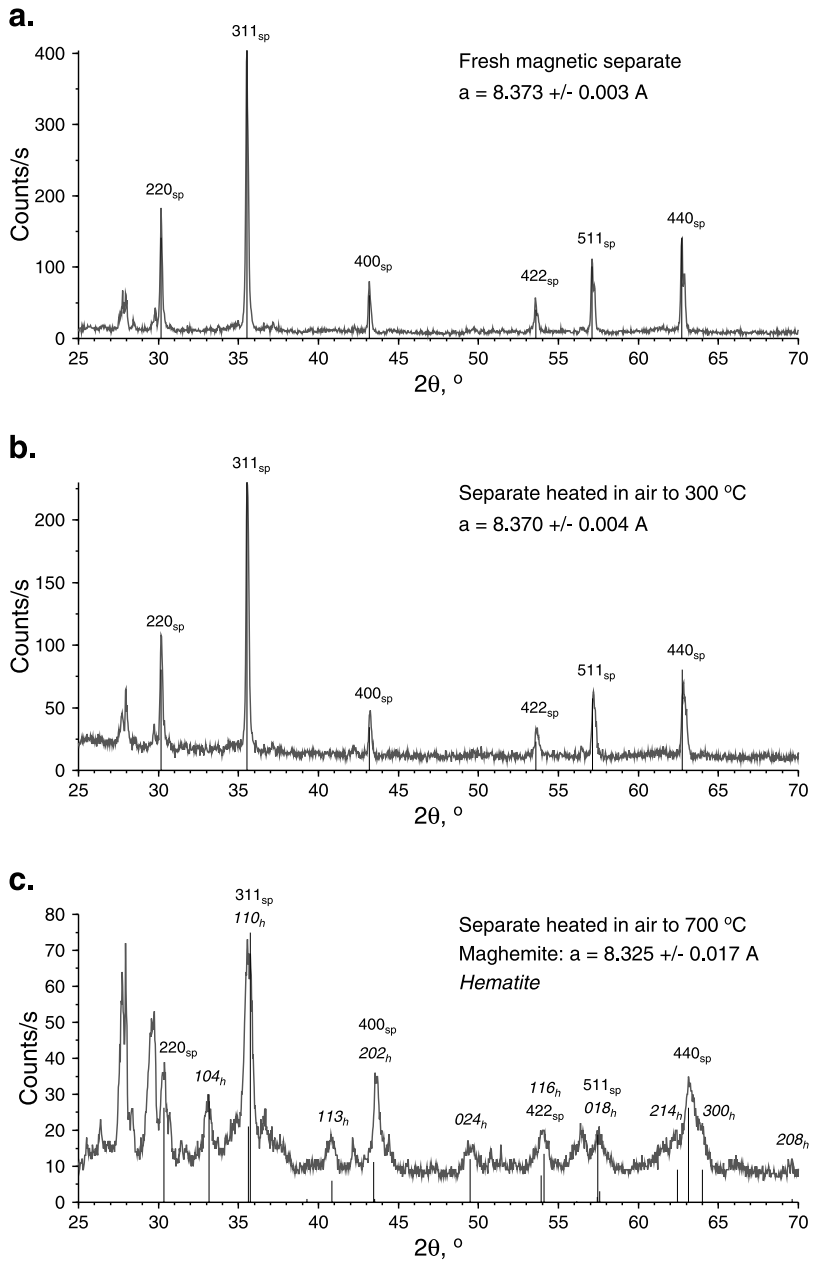

Figure 10. X-ray powder diffraction spectra measured (a) from fresh magnetic separate and from separates heated in air to (b) 300°C and (c) 700°C for sample 803D-68R4-42.

heating to 300°C); for sample 1187A-6R3-44, the decrease was from 8.352 ± 0.005 Å (fresh) to 8.346 ± 0.004 Å (heated to 325°C).

[57] Upon further heating, the titanomaghemite in these samples apparently breaks up to form complex multiphase assemblages of inversion products. In the X-ray spectra measured from separates heated to 700°C (Figure 10c), diffraction lines become broad and weak, consistent with greatly reduced "diffractive power" of the inversion product phases due to their small effective grain sizes. Diffraction lines from hematite and maghemite ($a = 8.33 \pm 0.02$ Å; the large uncertainty allows for the line broadening and peak overlaps) were observed in the spectra. Maghemite (rather than magnetite) is expected as an inversion product because of the initially high oxidation state of titanomaghemite and oxidizing conditions (heating in air). It does not completely invert to hematite upon heating to 700°C; examples of such "high-temperature stability of maghemite" have been reported [e.g., *Özdemir and Banerjee*, 1984]. We were not able to positively identify a Ti-rich inversion product phase. This may be because this phase is remote in compositional space from the original titanomaghemite (e.g., TiO_2), or it is in an amorphous/poorly crystalline form. (Note that the peaks, which do not correspond to hematite and maghemite in Figure 10c, are also seen in the spectrum from the fresh sample (Figure 10a). They originate from the contamination of the magnetic separates by silicate matrix material (plagioclase and clinopyroxene). Their "higher intensities" in Figure 10c are

deceptive because of the smaller peak intensities from the inversion product.)

[58] Although the 0.003–0.006 Å decrease in a upon heating to 300–325°C is comparable with the uncertainties of lattice parameter values, the consistently lower values for the heated samples suggest additional single-phase oxidation of titanomaghemite during heating in air. This, however, does not explain the irreversibility of $\kappa(T)$ curves upon heating to 300°C (Figure 9). *Özdemir and O'Reilly* [1982] showed that the magnetic susceptibility of highly oxidized synthetic titanomaghemites increases with the increasing z. The increase in z, which can be inferred from the decrease in lattice parameter ($\Delta z \approx 0.01$–0.02 for the 0.003–0.006 Ådecrease in a), does not seem to be sufficient to account for the observed increases in κ. This becomes even more problematic for the samples heated in an inert atmosphere (argon), which show greater increases in susceptibility upon heating to 300°C. A directly opposite situation (i.e., smaller irreversibility in argon runs) would be expected if single-phase oxidation were a major cause of irreversibility of $\kappa(T)$ curves up to 300°C.

[59] The more likely explanation is the onset of titanomaghemite inversion. We suggest that the inversion begins with nucleation of Ti-rich and Ti-poor spinel regions which conform to the cubic spinel structure of original titanomaghemite. This process can be viewed as unmixing of the original titanomaghemite into Ti-enriched and Ti-depleted titanomaghemite domains along a line nearly parallel to the line of constant lattice parameter (e.g., Figure 6). The chemical domains thus created have nearly the same a values as that of original phase, preserving the preexisting oxygen lattice. The creation of a metastable Fe-rich inversion product may be responsible for the increases in magnetic susceptibility upon heating to 300°C. The additional single-phase oxidation during heating in air, producing new lattice cells (oxidation by the addition of oxygen), and the necessity of redistributing newly created cation vacancies counteract the unmixing, stabilizing the cation-deficient structure of titanomaghemite and resulting in the smaller irreversibility of $\kappa(T)$ curves.

8. Discussion

8.1. ChRM Inclination Data

[60] The rock magnetic and compositional data presented in sections 5, 6, and 7 suggest that the NRM of basalts from the nine DSDP and ODP sites in the Pacific Ocean selected for this study is a single-domain to pseudosingle-domain chemical remanent magnetization (CRM) carried by titanomaghemite with P-type (and/or Q-type) thermomagnetic behavior, or by mixtures of titanomaghemite carriers with P-type behavior and N-type behavior with compensation temperatures below room temperature. This CRM is likely to inherit the direction of the parental thermoremanent magnetization of titanomagnetite [e.g., *Marshall and Cox*, 1971; *Özdemir and Dunlop*, 1985] and can be used as a characteristic remanent magnetization to define paleomagnetic directions.

[61] ChRM inclination data obtained from thermal demagnetization experiments in this study (section 4, Table 3) are generally consistent with inclination data previously reported [*Larson and Lowrie*, 1975; *Wallick and Steiner*, 1992; *Mikada et al.*, 2002; *Riisager et al.*, 2003]. The only significant discrepancy was observed between our data and data of *Larson and Lowrie* [1975], who reported an average inclination of $-11° \pm 1°$ from Site 303A basalt. Our data for all basalt samples from Site 303A show shallower, positive inclinations with an average value of 3.7° (Table 3). According to the magnetic anomaly identifications of *Larson and Lowrie* [1975], Site 303A is located on normally magnetized crust (chron M5n) formed in the southern hemisphere. Assuming that the Site 303A basalts are of the same age as the bulk oceanic profile, our estimate of the average ChRM inclination suggests a more northerly, nearly equatorial position of Site 303A in Early Cretaceous ($1.9° \pm 2.6°$ N) instead of a $5.8° \pm 0.5°$ S paleolatitude suggested by *Larson and Lowrie* [1975]. However, because the short sequence of the Site 303A basalts probably represents a single cooling unit (a stack of basaltic pillows [*Marshall*, 1975]) which does not average the secular variation of geomagnetic field, both estimates may be inaccurate. For example, if we consider low-latitude sites ($\leq 20°$) for the 110–195 Ma interval, a $\sim 29°$ angular dispersion of paleomagnetic directions is predicted at the equator [*McFadden et al.*, 1991]. Similarly, the ChRMs (Table 3) of the other short sections (sites 170, 304, 803D, and 1173B) should not be used to calculate paleolatitudes, because the stratigraphic sequences from these sites lack the clear geological indicators of elapsed time present at other sites (see discussion by *Tarduno and Sager* [1995]).

[62] Because only twelve samples of the tholeiitic basalt sequence from Site 801C were demagnetized (and half of these samples did not yield a stable ChRM), we were not able to positively correlate the changes of the ChRM inclination and polarity with data previously reported from the Site 801C sequence [*Wallick and Steiner*, 1992]. We note, however, that on a sample basis our ChRM inclination data are in a good agreement with the results of *Wallick and Steiner* [1992] (auxiliary material Table S1). The Site 801C basalts were erupted during the Jurassic Quiet Zone characterized by very rapid polarity changes [*Opdyke and Channell*, 1996; *Tivey et al.*, 2005]. *Wallick and Steiner* [1992] interpreted their data from the upper 60 meters at Site 801C as representing at least five reversal of geomagnetic polarity. It was also suggested that some of the basalt samples from Site 801C may have recorded transitional geomagnetic directions, which is consistent with a large scatter of the absolute values of ChRM inclination. Because of these limitations and our selective sampling, we did not attempt to calculate an average inclination from the Site 801C inclination data.

8.2. Origin of the Apparent Antiparallel NRM Components in Thermal Demagnetization Data

[63] Alternating field demagnetization data and pTRM acquisition experiments (sections 4 and 5) suggest that the apparent antiparallel magnetization components observed upon thermal demagnetization in some highly oxidized basalt samples from sites 303A, 801C, 803D, 1185B, and 1187A do not represent the unblocking of true self-reversed CRM components carried by titanomaghemite with N-type thermomagnetic behavior above room temperature. This interpretation is consistent with the titanomaghemite compositions (section 6), which show either lower oxidation

states (sites 303A, 801C, and 803D) or x values (sites 1185B and 1187A) than those observed in self-reversing titanomaghemites from the Detroit Seamount basalts [*Doubrovine and Tarduno*, 2004].

[64] Remarkably, the increases of the NRM intensity upon thermal demagnetization to ~200–350°C were most common in the basalts from Site 1187A. Titanomaghemite in the Site 1187A basalts (and in the Site 1185B basalts) showed the highest oxidation states ($z \geq \sim 0.9$, section 6.2) but low Ti contents ($0.30 \leq x \leq 0.56$, section 6.1). Because the magnetization of titanomaghemite with $x < 0.6$ is dominated by the B magnetic sublattice at any oxidation state [*Verhoogen*, 1962; *O'Reilly and Banerjee*, 1966], it is not possible for low-Ti titanomaghemite to undergo the self-reversal by ionic reordering. The self-reversal explanation of the apparent antiparallel NRM components in the basalts from sites 1185B and 1187A can thus be ruled out on the basis of titanomaghemite composition.

[65] From the similarities in thermal demagnetization behavior and rock magnetic properties of the samples from sites 1185B and 1187A and the basalts containing titanomaghemites with higher x values and showing the apparent antiparallel NRM components (sites 303A, 801C, and 803D), it seems likely that a common process is responsible for the increases of the NRM intensity seen in a ~200–350°C range of unblocking temperatures, irrespectively of the Ti content of titanomaghemite. The actual mechanism is not clear, and different explanations can be considered.

8.2.1. Inversion of Titanomaghemite

[66] A typical assumption to explain the antiparallel magnetization components observed upon thermal demagnetization would invoke the thermally induced inversion of titanomaghemite and magnetostatic or exchange interactions in the multiphase inversion products [e.g., *Creer et al.*, 1970]. Depending on the sign of the assumed interactions, either a thermally induced self-reversal (negative coupling) followed by the unblocking of the self-reversed magnetization, or positive coupling within the inversion product, may produce an increase of the NRM intensity in the intermediate range of unblocking temperatures. Titanomaghemite inversion was suggested to be responsible for the apparent "self-reversed NRM components" observed in thermal demagnetization experiments in some prior studies of submarine basalts [*Mayer and Tarduno*, 1993; *Riisager et al.*, 2003]. This explanation, however, requires the formation of multiphase inversion products at or below the unblocking temperatures of "the reversed NRM component."

[67] In our samples showing "the reversed NRM components," the onset of titanomaghemite inversion was observed between 250 and 300°C (sections 7.2 and 7.3). The increases in the NRM intensity in thermal demagnetization data were seen after heatings to slightly lower temperatures, usually starting at 225–250°C and sometimes at temperatures as low as 175–200°C (auxiliary material Table S1). The development of multiphase inversion products at (or below) these relatively low temperatures is not consistent with nearly reversible $\kappa(T)$ curves measured in the heating-cooling cycles with the 200–250°C maximum temperatures (section 7.3). Moreover, the heating experiments on magnetic separates (section 7.4) suggest that the oxygen face-centered cubic lattice of titanomaghemite remains largely intact after heating to the maximum unblocking temperature of "the reversed NRM component"; the small decreases in lattice parameter observed for the magnetic separates heated in air to 300–325°C are consistent with additional single-phase oxidation, which apparently dominates the alteration of titanomaghemite below ~250°C.

[68] As it was discussed in section 7.4, the formation of the metastable Fe-rich spinel phase begins between 250 and 300°C, presumably due to the nucleation of minute Fe- and Ti-enriched compositional domains, preserving the oxygen lattice of the initial titanomaghemite. Physical separation of these chemically heterogeneous but crystallographically coherent particles into magnetically interacting Fe-rich spinel regions (and nonspinel phases) probably occurs above the maximum unblocking temperatures of "the reversed NRM components," as suggested by greatly increased irreversibility of the $\kappa(T)$ curves upon heating to 400–500°C (Figure 9) and by the X-ray data from the heated magnetic separates (Figure 10). These temperatures are in good agreement with the "inversion temperatures" reported from highly oxidized synthetic titanomaghemites (i.e., inversion temperatures $\geq$400°C for titanomaghemites with $x = 0.6$ and $z > 0.8$) [*Özdemir*, 1987]. Thus it seems unlikely that the unmixing of titanomaghemite into magnetically interacting assemblages of the inversion products could produce the increases of the NRM intensity upon heating to ~200–350°C.

8.2.2. Magnetostatic Interactions

[69] *Krása* [2003] and *Krása et al.* [2005] reported a partial self-reversal of magnetization in samples of continental basalts containing inhomogeneously oxidized titanomaghemite. They suggested that the self-reversal originated from negative magnetostatic interactions between more and less oxidized regions of inhomogeneously oxidized titanomaghemite grains; this interpretation is consistent with the reported rock magnetic data and was supported by the results of micromagnetic calculations [*Krása et al.*, 2005]. A similar mechanism can be invoked to explain our data. The decrease in lattice parameter during progressive low-temperature oxidation of titanomagnetite is accommodated by the development of "shrinkage cracks," which may subdivide single grains of titanomaghemite into assemblages of physically separated subgrains. Skeletal shapes of titanomagnetite grains, which were typically observed in our samples, make such subdivision even more likely. In a magnetostatically interacting assemblage of subgrains, subgrains unblocked at a certain temperature may acquire a TRM in a backfield of subgrains which remain blocked. If the magnetostatic coupling is negative, i.e., the subgrains with lower unblocking temperature acquire magnetization (M_1) in the direction nearly opposite to that of the blocked subgrains (M_2), a partial (if $M_1 < M_2$) or complete (if $M_1 > M_2$) self-reversal will result. Both partial and complete self-reversals due to magnetostatic interactions were reported [*Krása*, 2003; *Krása et al.*, 2005].

[70] In stepwise thermal demagnetization experiments, the partial self-reversal of magnetization will produce a sharp decrease in the NRM intensity at temperatures where the reversed TRM is blocked; the complete self-reversal will reverse the NRM direction. None of these were observed in our data. However, if the magnetostatically interacting

assemblages represent only a small fraction of remanence carriers, the complete self-reversal in interacting subgrains (combined with a steady decrease of the NRM carried by noninteracting grains) will first result in a decrease of NRM due to the blocking of self-reversed magnetization, and then in an increase of the NRM intensity at temperatures where the entire interacting assemblages get unblocked. The further decrease of the NRM intensity is due to unblocking of noninteracting grains. This qualitative explanation is consistent with thermal demagnetization data from the most samples showing the apparent antiparallel NRM components, as well as with the AF demagnetization and pTRM acquisition data. *Krása et al.* [2005] showed that fields as low as 10 μT are sufficient to completely suppress the self-reversal; a 40 μT field was used in our pTRM acquisition experiments. This simple mechanism, however, does not explain the thermal demagnetization behavior of the samples which show only a small decrease of the NRM intensity below $\sim$200°C followed by an increase upon heating to $\sim$200–350°C (e.g., Figure 3i). It also ignores the effect of compositional and microstructural changes associated with the onset of inversion in titanomaghemite.

8.2.3. Single-Phase Oxidation

[71] Recently, we reported similar thermal demagnetization data from the basalt samples collected at DSDP Site 307 and suggested that the additional single-phase oxidation of titanomaghemite (which pushes its composition into the compositional field where the self-reversal by ionic reordering is possible) may be responsible for the increases of NRM intensity upon heating to $\sim$200–300°C [*Doubrovine and Tarduno*, 2005]. Our new data (sections 7.3 and 7.4) suggest that while single-phase oxidation tend to stabilize the cation-deficient structure of titanomaghemite, titanomaghemite nevertheless begins to unmix between 250 and 300°C. Moreover, single-phase oxidation alone cannot shift the compositions of low-Ti titanomaghemites (sites 1185B and 1187A) into the self-reversal field.

[72] The unmixing of titanomaghemite into the metastable Ti-rich and Fe-rich spinel inversion products (as suggested by the X-ray data from heated magnetic separates and $\kappa(T)$ curves, sections 7.3 and 7.4) may create Ti-enriched titanomaghemite with a composition within the self-reversal field, even from the initial low-Ti titanomaghemite. This process may result in the development of a self-reversed CRM component; the unblocking of this CRM in the intermediate temperature range may produce an increase of the NRM intensity. This explanation, however, suffers from the same limitation as that for "the inversion explanation" discussed above: the unmixing has to occur at or below the unblocking temperatures of "the reversed NRM component."

[73] Although the unmixing into Ti- and Fe-enriched spinel regions probably occurs at the earliest stages of the titanomaghemite inversion, corresponding to the 250–300°C range of the inversion onset, these temperatures are some 25–50°C higher than the minimum heating temperatures after which the NRM intensity begins to increase for the majority of the samples showing the apparent antiparallel NRM components (auxiliary material Table S1). Because the prolonged, repeat heatings in air during thermal demagnetization experiments ($\sim$40 min per each demagnetization step) may facilitate the onset of inversion at temperatures lower than those observed from thermomagnetic curves, we cannot completely rule out "the unmixing explanation" of the apparent antiparallel NRM components. We note, however, that the degrees of irreversibility seen in the $\kappa(T)$ runs up to 200–250°C (Figure 9) seem to be inconsistent with significant unmixing at these or lower temperatures.

8.2.4. In Situ Ionic Reordering

[74] The mechanisms discussed above fail to adequately explain all available data. Magnetostatic coupling in physically subdivided titanomaghemite grains, although consistent with the majority of observations, requires rather fortuitous subgrain arrangements, with smaller subgrains having higher unblocking temperatures than those of the larger subgrains, which seems counterintuitive. We cannot completely rule out the possibility that highly oxidized titanomaghemites with "normally high" x values (from the Site 303A, 801C and 803D basalts) may carry small self-reversed CRM components formed in situ due to ionic reordering in titanomaghemite. However, this is not supported by the pTRM and high-field thermomagnetic data, and requires invoking a different mechanism to explain very similar thermal demagnetization behavior of some samples from the Site 1185B and 1187A basalts.

8.3. Experimental Definition of the Titanomaghemite Self-Reversal Field

[75] In this section, we compile available data on compositions of titanomaghemite from moderately to highly oxidized oceanic and continental basalts, for which the temperature dependences of saturation magnetization and/or self-reversals of laboratory-imparted remanent magnetizations were reported. Specifically, we selected data from basalts showing P-type and N-type thermomagnetic properties [*Schult*, 1968, 1971, 1976; *Matzka et al.*, 2003; *Doubrovine and Tarduno*, 2004, 2005, 2006]. The average titanomaghemite compositions were estimated from the reported microanalytical data (x values), Curie temperatures and lattice parameters using the reference contours of *Readman and O'Reilly* [1972]. Because the degrees of cation substitution were not reported in the majority of these studies, we calculated x and z values assuming no cation substitution; these values are only tentative. For samples, from which microanalytical data were available [*Schult*, 1968, 1976; *Doubrovine and Tarduno*, 2004, 2005, 2006], the x values were calculated using equation (1). The x values and lattice parameters [*Schult*, 1976; *Doubrovine and Tarduno*, 2004, 2005, 2006] or Curie temperatures [*Schult*, 1968] were used to estimate z. For samples of *Matzka et al.* [2003], the x and z values were calculated from the reported lattice parameters and Curie temperatures.

[76] All compositional data were divided into two groups: those from the samples showing P-type thermomagnetic behavior, and those from the samples showing N-type ferromagnetism. Only the samples showing self-reversals of laboratory-imparted magnetizations (SIRM, pTRM) or NRM due to N-type magnetization were considered as those representing N-type magnetic carriers. The remaining samples were considered as P-type, even in cases when the M_s minima were observed at cryogenic temperatures in the high-field thermomagnetic curves [e.g., *Matzka et al.*, 2003]. Such "minima" may correspond to the magnetic ordering of ilmenite or high-Ti hemoilmenite. We

did not discriminate between L-type and P-type properties; the data from samples which were described by *Schult* [1968] as those showing L-type thermomagnetic behavior were considered to be the P-type curves, because the original interpretation of L-type behavior was based on extrapolation from 77 K to 0 K.

[77] The compositions of titanomaghemite in basalt samples showing P-type and N-type thermomagnetic properties are shown in Figure 11. The two compositional ranges overlap considerably, suggesting that both P-type and N-type magnetic carriers may correspond to the same "nominal composition" (i.e., the composition estimated from the bulk magnetic and analytical data, ignoring the effect of cation impurities). In fact, the only average compositions from the basalts with N-type thermomagnetic properties, which do not fall into the P-type compositional range, are those from the self-reversing samples of the Detroit Seamount basalt [*Doubrovine and Tarduno*, 2004]. There are several reasons which may result in such overlap.

[78] Because the same data set of *Readman and O'Reilly* [1972] was used to estimate the compositions, we do not expect that possible errors in the reference data can contribute significant scatter into the calculated values. Similarly, if the degrees of cation substitution are approximately the same for all samples, the neglect of the influence of cation impurities will affect all data in the similar way: the estimates of z and x will be systematically higher, resulting in a similar overlap in the "corrected data." On the other hand, varying amounts of the cation impurities will introduce scatter into the data. A significant variation in δ_{Al} and δ_{Mg} was observed in our compositional data from the nine Pacific sites (Table 2).

[79] On the basis of the comparison of the compositional and rock magnetic data from titanomaghemites from the DSDP sites 166 and 307 [*Doubrovine and Tarduno*, 2006], we suggested that if the magnetic carrier is represented by mixtures of grains with P- and N-type behavior, the values estimated from bulk compositional data may be biased toward the compositions of the large, least oxidized grains with P-type thermomagnetic properties. Mixed P- and N-type carriers may be the case for all basalts in the "N-type group" (Figure 11). While the N-type self-reversal is the only unequivocal evidence for N-type magnetism, this criterion does not distinguish whether the N-type carriers are the only magnetic carriers within a sample. This may explain why the values from the two least oxidized samples from the Steinberg at Meensen basalt [*Schult*, 1976] fall below the theoretical self-reversal field of *O'Reilly and Banerjee* [1966], while the compositions from the remaining N-type titanomaghemites are in good agreement with this field. We note that all samples of the Steinberg at Meensen basalt come form a single ~10-cm-large hand specimen, in which a pronounced core-to-surface oxidation gradient was observed [*Schult*, 1976]; a significant variability of the titanomaghemite oxidation state can thus be expected in these samples.

[80] In the theoretical model, *O'Reilly and Banerjee* [1966] considered an idealized situation, assuming that all cation vacancies reside in the octahedral (B) crystallographic sites. However, if some vacancies remain in the tetrahedral (A) sublattice, the titanomaghemites with compositions slightly above the lower boundary of the theoretical self-reversal field will have P-type thermomagnetic properties, rather than N-type properties. This may explain why the compositions of titanomaghemite from the Site 303A, 803D and 307 basalts are within the theoretical compositional limits of self-reversal by ionic reordering (Figure 11).

[81] All of the reasons discussed above probably contribute to the observed overlap of the P-type and N-type compositional ranges (Figure 11). Given the quality of the available compositional data, and, more importantly, the inevitable natural variability of compositional parameters (x, degrees of cation substitution, z) within a sample, it does not seem possible to constrain the boundary between the P- and N-type compositions of titanomaghemite from the available experimental data (and hence the self-reversal field) more precisely than it has been done in Figure 11. The P-N boundary may be viewed as a "compositional band" where P-type, N-type, or a combination of the two may be observed. (Although it should be stressed that the "composition" is the average nominal value, estimated as described above.) We chose the band so that the theoretical P-N boundary of *O'Reilly and Banerjee* [1966] bisects it. Because of the limited data, the band is essentially unconstrained at $x \geq \sim 0.8$ and $z \leq \sim 0.5$.

[82] Compositions of titanomaghemite from the Steinberg at Meensen basalt [*Schult*, 1976] and the Detroit Seamount basalts suggest that the minimum oxidation state which may produce a self-reversed CRM in single-domain titanomaghemite with $x \geq 0.65$ is $z \geq 0.86$ [*Schult*, 1976] or $z \geq 0.95$ [*Doubrovine and Tarduno*, 2004]. New titanomaghemite compositional data from the Site 303A and 803D basalts, which showed either P-type thermomagnetic behavior (Site 803D) or thermomagnetic properties consistent with mixed P-type magnetic carriers and N-type carriers with compensation temperatures below room temperature (Site 303A) support the higher limit ($z \geq 0.95$). Because extremely high oxidation states are required, and these oxidation degrees were not observed even in samples representing the highest degrees of overall basalt alteration (e.g., sites 801C and 803D), the self-reversal of NRM by ionic reordering in titanomaghemite is probably not a common characteristic of oceanic basalts. Instead, it appears that special conditions (e.g., extreme fluid flow) may be needed to reach these high oxidation states at low temperature.

9. Conclusions

[83] In our survey of DSDP and ODP basalt samples with demonstrable evidence of seafloor weathering (as defined by alteration mineralogy) we have defined two types of reversed polarity magnetization components: (1) an apparently rare partial self-reversed component of natural remanent magnetization related to ionic reordering during low-temperature oxidation of titanomaghemite and (2) a more common reversed component that is apparent only is thermal demagnetization studies.

[84] The latter type of reversed component has been described in some prior studies. At unblocking temperatures between approximately 200 and 350°C, a magnetization component exactly reversed to that isolated at lower or higher unblocking temperatures is isolated. Our analyses indicate that this component is not related to N-type grains produced in nature. However, we also conclude that the oft assumed

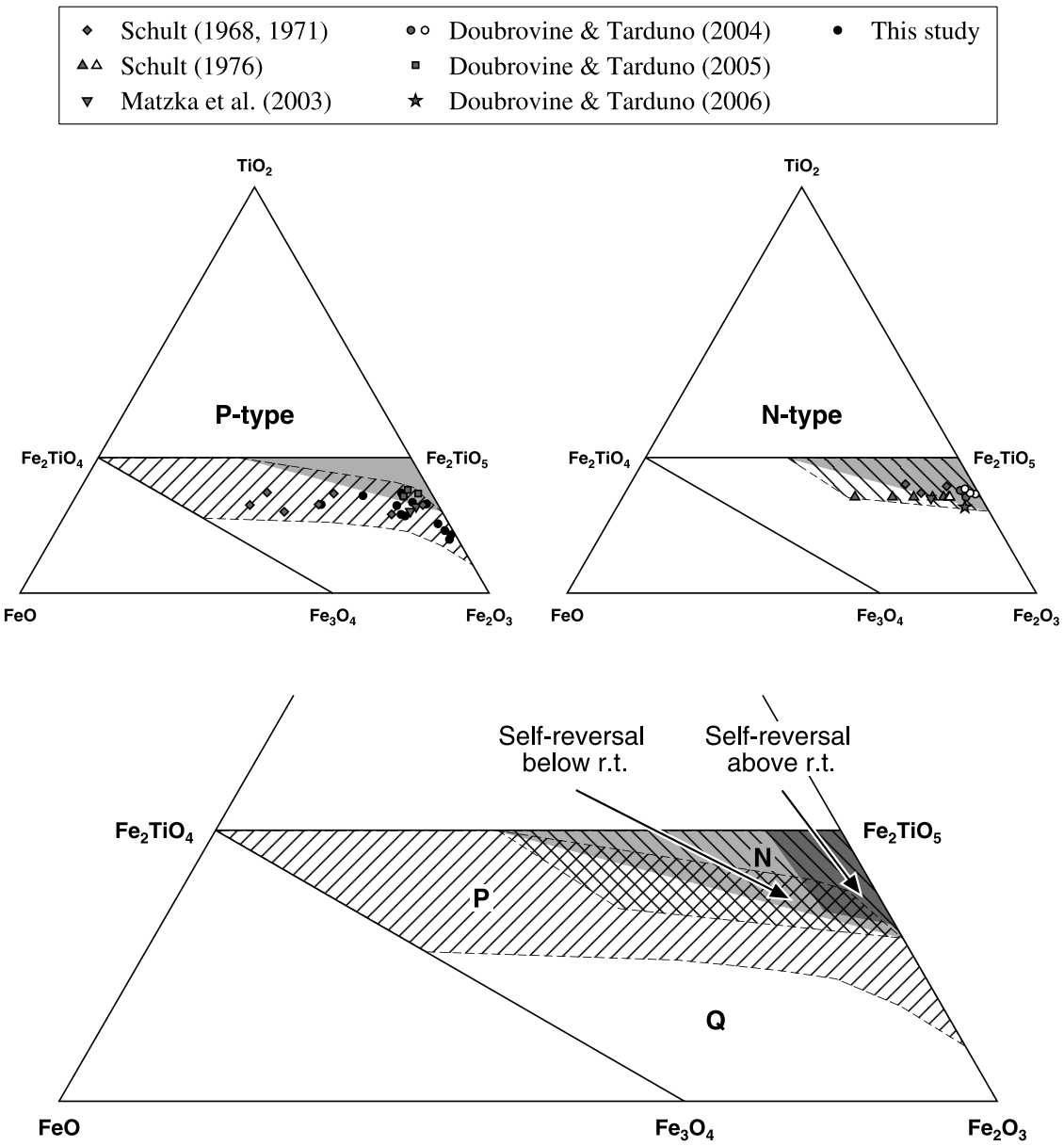

Figure 11. TiO_2-FeO-Fe_2O_3 ternary diagrams showing the compositional data from natural titanomaghemites with P-type and N-type thermomagnetic behavior (top left and top right diagrams, respectively), and self-reversal fields (bottom). Light gray area is the self-reversal field of *O'Reilly and Banerjee* [1966]. Dark gray area is the proposed field of self-reversal above room temperature.

mechanism of titanomagnetite inversion and exchange or magnetostatic interactions between newly created magnetic phases is inadequate to fully explain the origin of this component. In particular, the unblocking temperature at which the component first appears is relatively low, compared to that at which large changes in magnetic mineralogy occur. Alternative mechanisms, including magnetostatic interaction and single phase oxidation (i.e., in situ production of N-type grains during laboratory heating) may play an important role in the complex set of transformations that likely accompany the thermal alteration of titanomaghemite at intermediate temperatures.

[85] We observed true self-reversed components above room temperature at only a single site, although a few sites show similar behavior below room temperature due to the presence of N-type grains. The available rock magnetic, XRD and SEM data allow us to constrain the compositions of titanomaghemite carrying self-reversed NRM components to very high oxidation states ($z > 0.9$) and high Ti contents ($x > 0.6$). Because of these severe requirements, the acquisition of self-reversed components during seafloor weathering is not likely to be a major factor controlling the amplitude of marine magnetic anomalies. On the other hand, the achievement of these high oxidation states by titanomagnetite, once thought unlikely because it would require temperatures too high to be consistent with maintaining the stability of the cation-deficient titanomagnetite lattice, can apparently occur in natural marine settings.

These appear to mark areas of fluid flow and concomitant Fe removal, resulting in high oxidation states at low temperature. Defining environments in the ocean basins where this might preferentially occur may be of potential future interest.

[86] **Acknowledgments.** This research used samples provided by the ODP. The ODP is supported by the U.S. National Science Foundation and participating countries under management of the Joint Oceanographic Institutions. We thank Brian McIntyre for his assistance with SEM and EDS analyses and Christine Pratt for X-ray data. We are grateful to the Institute for Rock Magnetism (IRM) for the use of their equipment. The IRM is funded by Keck Foundation, the U.S. National Science Foundation, and the University of Minnesota. P.D. appreciates a visiting fellowship from the IRM and wishes to thank Mike Jackson and Peat Sølheid for the help during his visit to the IRM. We thank David Krása, Freidrich Heller, and Wyn Williams for reviews of the manuscript.

References

Alt, J. C., and D. A. H. Teagle (2003), Hydrothermal alteration of upper oceanic crust formed at a fast-spreading ridge: Mineral, chemical, and isotopic evidence from ODP Site 801, *Chem. Geol.*, *201*, 191–211.

Banerjee, N. R., and J. Honnorez (2004), Data report: Low-temperature alteration of upper oceanic crust from the Ontong Java Plateau, Leg 192: Alteration and vein logs, *Proc. Ocean Drill. Program Sci. Results, 192*[Online], 8 pp. (Available at http://www-odp.tamu.edu/publications/192_SR/VOLUME/CHAPTERS/103.PDF).

Bleil, U., and N. Petersen (1983), Variations in magnetization intensity and low-temperature titanomagnetite oxidation of ocean floor basalts, *Nature*, *301*, 384–388.

Brown, K., and W. O'Reilly (1988), The effect of low-temperature oxidation on the remanence of TRM-carrying titanomagnetite $Fe_{2.4}Ti_{0.6}O_4$, *Phys. Earth Planet. Inter.*, *52*, 108–116.

Carvallo, C., Ö. Özdemir, and D. J. Dunlop (2004), Palaeointensity determinations, palaeodirections and magnetic properties of basalts from the Emperor seamounts, *Geophys. J. Int.*, *156*, 29–38.

Chambers, L. M., M. S. Pringle, and J. G. Fitton (2004), Phreatomagmatic eruptions on the Ontong Java Plateau: An Aptian $^{40}Ar/^{39}Ar$ age for volcaniclastic rocks at ODP Site 1184, in *Origin and Evolution of the Ontong Java Plateau*, edited by J. G. Fitton et al., *Geol. Soc. Spec. Publ.*, *229*, 325–331.

Creer, K. M., and J. D. Ibbetson (1970), Electron microprobe analyses and magnetic properties of non-stoichiometric titanomagnetites in basaltic rocks, *Geophys. J. R. Astron. Soc.*, *21*, 485–511.

Creer, K. M., N. Petersen, and J. Petherbridge (1970), Partial self-reversal of remanent magnetization and anisotropy of viscous magnetization in basalts, *Geophys. J. R. Astron. Soc.*, *21*, 471–483.

Day, R., M. D. Fuller, and V. A. Schmidt (1977), Hysteresis properties of titanomagnetites: Grain size and composition dependence, *Phys. Earth Planet. Inter.*, *13*, 260–267.

Doubrovine, P. V., and J. A. Tarduno (2004), Self-reversed magnetization carried by titanomaghemite in oceanic basalts, *Earth Planet. Sci. Lett.*, *222*, 959–969.

Doubrovine, P. V., and J. A. Tarduno (2005), On the compositional field of self-reversing titanomaghemite: Constraints from Deep Sea Drilling Project Site 307, *J. Geophys. Res.*, *110*, B11104, doi:10.1029/2005JB003865.

Doubrovine, P. V., and J. A. Tarduno (2006), N-type magnetism at cryogenic temperatures in oceanic basalt, *Phys. Earth Planet. Inter.*, *157*, 46–54.

Dunlop, D. J. (2002), Theory and application of the Day plot (M_{rs}/M_s versus H_{cr}/H_c): 1. Theoretical curves and tests using titanomagnetite data, *J. Geophys. Res.*, *107*(B3), 2056, doi:10.1029/2001JB000486.

Dunlop, D. J., and Ö. Özdemir (1997), *Rock Magnetism, Fundamentals and Frontiers*, 573 pp., Cambridge Univ. Press, New York.

Fabian, K. (2006), Approach to saturation analysis of hysteresis measurements in rock magnetism and evidence for stress dominated magnetic anisotropy in young mid-ocean ridge basalt, *Phys. Earth Planet. Inter.*, *154*, 299–307.

Furuta, T. (1993), Magnetic properties and ferromagnetic mineralogy of ocean basalts, *Geophys. J. Int.*, *113*, 95–114.

Goldstein, J. I., A. D. Romig Jr., D. E. Newbury, C. E. Lyman, P. Echlin, C. Fiori, D. C. Joy, and E. Lifshin (1992), *Scanning Electron Microscopy and X-Ray Microanalysis: A Text for Biologists, Material Scientists, and Geologists*, 820 pp., Springer, New York.

Gradstein, F. M., et al. (2004), *A Geologic Time Scale 2004*, 589 pp., Cambridge Univ. Press, New York.

Hoffman, K. A. (1982), Partial self-reversal in basalts containing mildly low-temperature oxidized titanomagnetite, *Phys. Earth Planet. Inter.*, *30*, 357.

Kirschvink, J. L. (1980), The least-squares line and plane and the analysis of paleomagnetic data, *Geophys. J. R. Astron. Soc.*, *62*, 699–718.

Krása, D. (2003), Self-reversal of remanent magnetisation of basalts—Origin, mechanisms and consequences, Ph.D. thesis, Fak. für Geowis., Ludwig-Maximilians-Univ., Munich, Germany.

Krása, D., V. P. Shcherbakov, T. Kunzmann, and N. Petersen (2005), Self-reversal of remanent magnetization in basalts due to partially oxidized titanomagnetites, *Geophys. J. Int.*, *162*, 115–136.

Kroenke, L. W., W. H. Berger, T. R. Janecek, and the Shipboard Scientific Party (1991), *Proceedings of the Ocean Drilling Program, Initial Reports*, vol. 130, Ocean Drill. Program, College Station, Tex.

Lancelot, Y., R. L. Larson, and the Shipboard Scientific Party (1990), *Proceedings of the Ocean Drilling Program, Initial Reports*, vol. 129, Ocean Drill. Program, College Station, Tex.

Larson, R. L., and W. Lowrie (1975), Paleomagnetic evidence for motion of the Pacific plate from Leg 32 basalts and magnetic anomalies, *Initial Rep. Deep Sea Drill. Proj.*, *32*, 571–577.

Larson, R. L., R. Moberly, and the Shipboard Scientific Party (1975), *Initial Reports of the Deep Sea Drilling Project*, vol. 32, U. S. Govt. Print. Off., Washington, D. C.

Mahoney, J. J., M. Storey, R. A. Duncan, K. J. Spencer, and M. Pringle (1993), Geochemistry and age of the Ontong Java Plateau, in *The Mesozoic Pacific: Geology, Tectonics, and Volcanism*, *Geophys. Monogr. Ser.*, vol. 77, edited by M. Pringle, W. W. Sager, and S. Stein, pp. 233–261, AGU, Washington, D. C.

Mahoney, J. J., J. G. Fitton, P. J. Wallace, and the Shipboard Scientific Party (2001), *Proceedings of the Ocean Drilling Program, Initial Reports*, vol. 192, Ocean Drill. Program, College Station, Tex.

Marshall, M. (1975), Petrology and chemical composition of basaltic rocks recovered on Leg 32, Deep Sea Drilling Project, *Initial Rep. Deep Sea Drill. Proj.*, *32*, 563–570.

Marshall, M., and A. Cox (1971), Effect of oxidation on the natural remanent magnetization in sub-oceanic basalt, *Nature*, *230*, 28–31.

Matzka, J., D. Krása, T. Kunzmann, A. Schult, and N. Petersen (2003), Magnetic state of 10–40 Ma old ocean basalts and its implications for implications for natural remanent magnetization, *Earth Planet. Sci. Lett.*, *206*, 541–553.

Mayer, H., and J. A. Tarduno (1993), Paleomagnetic investigation of the igneous sequence, Site 807, Ontong Java Plateau, and a discussion of Pacific true polar wander, *Proc. Ocean Drill. Program Sci. Results*, *130*, 51–59.

McFadden, P. L., and A. B. Reid (1982), Analysis of paleomagnetic inclination data, *Geophys. J. R. Astron. Soc.*, *69*, 307–319.

McFadden, P. L., R. T. Merrill, M. W. McElhinny, and S. Lee (1991), Reversals of the Earth's magnetic field and temporal variations of the dynamo families, *J. Geophys. Res.*, *96*, 3923–3933.

Mikada, H., K. Becker, J. C. Moore, A. Klaus, and the Shipboard Scientific Party (2002), *Proceedings of the Ocean Drilling Program, Initial Reports*, vol. 196, Ocean Drill. Program, College Station, Tex.

Moskowitz, B. M. (1980), Theoretical grain size limits for single-domain, pseudo-singe-domain and multi-domain behavior in titanomagnetite ($x = 0.6$) as a function of low-temperature oxidation, *Earth Planet. Sci. Lett.*, *47*, 285–293.

Nagata, T. (1961), *Rock Magnetism*, 2nd ed., 350 pp., Maruzen, Tokyo.

Néel, L. (1948), Propriétés magnétiques des ferrites; ferrimagnétisme et antiferromagnétisme, *Ann. Phys.*, *3*, 137–198.

Nishida, J., and S. Sasajima (1974), Examination of self-reversal due to N-type magnetization in basalt, *Geophys. J. R. Astron. Soc.*, *37*, 453–460.

Nishitani, T., and M. Kono (1983), Curie temperature and lattice constant of oxidized titanomagnetite, *Geophys. J. R. Astron. Soc.*, *74*, 585–600.

O'Donovan, J. B., and W. O'Reilly (1977), Range of non-stoichiometry and characteristic properties of the products of laboratory maghemitization, *Earth Planet. Sci. Lett.*, *34*, 291–299.

Opdyke, N. D., and J. E. T. Channell (1996), *Magnetic Stratigraphy*, 346 pp., Elsevier, New York.

O'Reilly, W. (1983), The identification of titanomaghemites: Model mechanisms for the maghemitization and inversion processes and their magnetic consequences, *Phys. Earth. Planet. Inter.*, *31*, 65–76.

O'Reilly, W. (1984), *Rock and Mineral Magnetism*, 220 pp., Blackie Acad. and Prof., New York.

O'Reilly, W., and S. K. Banerjee (1966), Oxidation of titanomagnetites and self-reversal, *Nature*, *211*(5044), 26–28.

Özdemir, Ö. (1987), Inversion of titanomaghemites, *Phys. Earth Planet. Inter.*, *46*, 184–196.

Özdemir, Ö., and S. K. Banerjee (1984), High temperature stability of maghemite (γ-Fe_2O_3), *Geophys. Res. Lett.*, *11*, 161–164.

Özdemir, Ö., and D. J. Dunlop (1985), An experimental study of chemical remanent magnetizations of synthetic monodomain titanomaghemites with initial thermoremanent magnetizations, *J. Geophys. Res.*, *90*, 11,513–11,523.

Özdemir, Ö., and W. O'Reilly (1981), Laboratory synthesis of aluminum-substituted titanomaghemites and their characteristic properties, *J. Geophys.*, *49*, 93–100.

Özdemir, Ö., and W. O'Reilly (1982), Magnetic hysteresis properties of synthetic monodomain titanomaghemites, *Earth Planet. Sci. Lett.*, *57*, 437–447.

Parkinson, I. J., B. F. Schaefer, the ODP Leg 192 Shipboard Scientists, and R. J. Arculus (2002), A lower mantle origin for the world's biggest LIP? A high precision Os isotope isochron from Ontong Java Plateau basalts drilled on ODP Leg 192, *Geochim. Cosmochim. Acta*, *66*, Suppl. A580.

Plank, T., J. N. Ludden, C. Escutia, and the Shipboard Scientific Party (2000), *Proceedings of the Ocean Drilling Program, Initial Reports*, vol. 185, Ocean Drill. Program, College Station, Tex.

Readman, P. W., and W. O'Reilly (1972), Magnetic properties of oxidized (cation-deficient) titanomagnetites (Fe, Ti, □)$_3$O$_4$, *J. Geomagn. Geoelectr.*, *24*, 69–90.

Richards, J. C. W., J. B. O'Donovan, Z. Hauptman, W. O'Reilly, and K. M. Creer (1973), A magnetic study of titanomaghemite substituted by magnesium and aluminum, *Phys. Earth Planet. Inter.*, *7*, 437–444.

Riisager, P., S. Hall, M. Antretter, and X. Zhao (2003), Paleomagnetic paleolatitude of Early Cretaceous Ontong Java Plateau basalts: Implications for Pacific apparent and true polar wander, *Earth Planet. Sci. Lett.*, *208*, 235–252.

Schult, A. (1965), Über die umkehr der remanenten magnetisierung von titanomagnetiten in basalten, *Beitr. Mineral. Petrogr.*, *11*, 196–216.

Schult, A. (1968), Self-reversal of magnetization and chemical composition of titanomagnetites in basalts, *Earth Planet. Sci. Lett.*, *4*, 57–63.

Schult, A. (1971), On the strength of exchange interactions in titanomagnetites and its relation to self-reversal, *J. Geophys.*, *37*, 357–365.

Schult, A. (1976), Self-reversal above room temperature due to N-type magnetization in basalt, *J. Geophys.*, *42*, 81–84.

Smirnov, A. V., and J. A. Tarduno (2000), Low-temperature magnetic properties of pelagic sediments (Ocean Drilling Program Site 805C): Tracers of maghemitization and magnetic mineral reduction, *J. Geophys. Res.*, *105*, 16,457–16,471.

Tarduno, J. A. (1990), Brief reversal polarity interval during the Cretaceous Normal Polarity Superchron, *Geology*, *18*, 683–686.

Tarduno, J. A., and W. W. Sager (1995), Polar standstill of the Mid-Cretaceous Pacific Plate and its geodynamic implications, *Science*, *269*, 956–959.

Tarduno, J. A., W. V. Sliter, T. J. Bralower, M. McWilliams, I. Premoli-Silva, and J. G. Ogg (1989), M-sequence reversals recorded in DSDP sediment cores from the western Mid-Pacific Mountains and Magellan Rise, *Geol. Soc. Am. Bull.*, *101*, 1306–1316.

Tarduno, J. A., W. V. Sliter, L. W. Kroenke, R. M. Leckie, H. Mayer, J. J. Mahoney, R. J. Musgrave, M. Storey, and E. L. Winterer (1991), Rapid formation of Ontong Java Plateau by Aptian mantle plume volcanism, *Science*, *254*, 399–403.

Tarduno, J. A., et al. (2003), The Emperor seamounts: Southward motion of the Hawaiian hotspot plume in Earth's mantle, *Science*, *301*, 1064–1069.

Tivey, M., R. Larson, H. Schouten, and R. Pockalny (2005), Downhole magnetic measurements of ODP Hole 801C: Implications for Pacific oceanic crust and magnetic field behavior in the Middle Jurassic, *Geochem. Geophys. Geosyst.*, *6*, Q04008, doi:10.1029/2004GC000754.

Verhoogen, J. (1956), Ionic reordering and self-reversal of magnetization in impure magnetites, *J. Geophys. Res.*, *61*(2), 201–209.

Verhoogen, J. (1962), Oxidation of iron-titanium oxides in igneous rocks, *J. Geol.*, *70*, 168–181.

von Dobeneck, T. (1996), A systematic analysis of natural magnetic mineral assemblages based on modelling hysteresis loops with coercivity-related hyperbolic basic functions, *Geophys. J. Int.*, *124*, 675–694.

Wallick, B. P., and M. B. Steiner (1992), Paleomagnetic and rock magnetic properties of Jurassic Quiet Zone basalts, Hole 801C, *Proc. Ocean Drill. Program Sci. Results*, *129*, 455–470.

Wang, D. (2002), Rock magnetic properties of young ocean-floor basalts during initial low-temperature alteration, *IRM Q.*, *12*(2), 4.

Winterer, E. L., J. I. Ewing, and the Shipboard Scientific Party (1973), *Initial Reports Deep Sea Drilling Project*, vol. 17, U. S. Govt. Print. Off., Washington, D. C.

Zhou, W., D. R. Peacor, R. Van der Voo, and J. F. Mansfield (1999), Determination of lattice parameter, oxidation state, and composition of individual titanomagnetite/titanomaghemite grains by transmission electron microscopy, *J. Geophys. Res.*, *104*(B8), 17,689–17,702.

P. V. Doubrovine and J. A. Tarduno, Department of Earth and Environmental Sciences, University of Rochester, Rochester, NY 14627, USA. (pavel@earth.rochester.edu; john@earth.rochester.edu)